5G Channel Model for bands up to100 GHz

Contributors:

Aalto University	**Nokia**
BUPT	**NTT DOCOMO**
CMCC	**New York University**
Ericsson	**Qualcomm**
Huawei	**Samsung**
INTEL	**University of Bristol**
KT Corporation	**University of Southern California**

Executive Summary

The future mobile communications systems are likely to be very different to those of today with new service innovations driven by increasing data traffic demand, increasing processing power of smart devices and new innovative applications. To meet these service demands the telecommunication industry is converging on a common set of 5G requirements which includes network speeds as high as 10 Gbps, cell edge rate greater than 100 Mbps and latency of less than 1msec. To be able to reach these 5G requirements the industry is looking at new spectrum bands in the range up to 100 GHz where there is spectrum availability for wide bandwidth channels.. For the development of the new 5G systems to operate in bands up to 100 GHz there is a need for accurate radio propagation models for these bands which are not addressed by existing channel models developed for bands below 6 GHz. This white paper presents a preliminary overview of the 5G channel models for bands up to 100 GHz. These have been derived based on extensive measurement and ray tracing results across a multitude of bands. The following procedure was used to derive the channel model in this white paper.

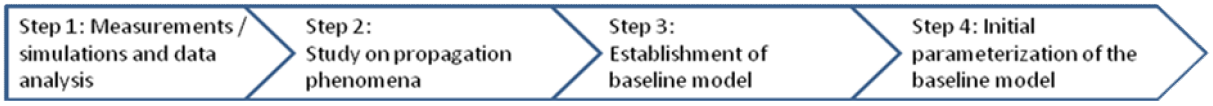

Based on extensive measurements and ray tracing across frequency bands from 6 GHz to 100 GHz, the white paper describes an initial 3D channel model which includes:

a. Typical deployment scenarios for urban micro (UMi), urban macro (UMa) and indoor (InH) environments.

b. A baseline model incorporating pathloss, shadow fading, line of sight probability, penetration and blockage models for the typical scenarios

c. Preliminary fast fading models for the above scenarios

d. Various processing methodologies (e.g. clustering algorithm, antenna decoupling etc.)

These studies have found some extensibility of the existing 3GPP models (e.g. 3GPP TR36.873) to the higher frequency bands up to 100 GHz. The measurements indicate that the smaller wavelengths introduce an increased sensitivity of the propagation models to the scale of the environment and show some frequency dependence of the path loss as well as increased occurrence of blockage. Further, the penetration loss is highly dependent on the material and tends to increase with frequency. The shadow fading and angular spread parameters are larger and the boundary between LOS and NLOS depends not only on antenna heights but also on the local environment. The small-scale characteristics of the channel such as delay spread and angular spread and the multipath richness is somewhat similar over the frequency range, which is encouraging for extending the existing 3GPP models to the wider frequency range.

While further work needs to be carried out to develop a complete channel model at these higher frequency bands, this white paper presents the first steps for an initial basis for the model

development.

Contents

1 Introduction

Next generation 5G cellular systems will encompass frequencies from around 500 MHz all the way to around 100 GHz. For the development of the new 5G systems to operate in bands above 6 GHz, there is a need for accurate radio propagation models for these bands which are not fully modelled by existing channel models below 6 GHz.. Previous generations of channel models were designed and evaluated for operation at frequencies only as high as 6 GHz. One important example is the recently developed 3D-urban micro (UMi) and 3D-urban macro (UMa) channel models for LTE [3GPP TR36.873]. The 3GPP 3D channel model provides additional flexibility for the elevation dimension, thereby allowing modeling two dimensional antenna systems, such as those that are expected in next generation system deployments. It is important for future system design to develop a new channel model that will be validated for operation at higher frequencies (e.g., up to 100 GHz) and that will allow accurate performance evaluation of possible future technical specifications for these bands over a representative set of possible environments and scenarios of interest. Furthermore, the new models should be consistent with the models below 6 GHz. In some cases, the requirements may call for deviations from the modelling parameters or methodology of the existing models, but these deviations should be kept to a bare minimum and only introduced when necessary for supporting the 5G simulation use cases.

There are many existing and ongoing campaign efforts worldwide targeting 5G channel measurements and modeling. They include METIS202 [METIS 2015], COST2100/COST[COST], IC1004 [IC], ETSI mmWave SIG [ETSI 2015], 5G mmWave Channel Model Alliance [NIST], MiWEBA [MiWEBA 2014], mmMagic [mmMagic], and NYU WIRELESS [Rappaport 2015, MacCartney 2015, Rappaport 2013, Samimi 2015]. METIS2020, for instance, has focused on 5G technologies and has contributed extensive studies in terms of channel modelling. Their target requirements include a wide range of frequency bands (up to 86 GHz), very large bandwidths (hundreds of MHz), fully three dimensional and accurate polarization modelling, spherical wave modelling, and high spatial resolution. The METIS channel models consist of a map-based model, stochastic model, and a hybrid model which can meet requirement of flexibility and scalability. The COST2100 channel model is a geometry-based stochastic channel model (GSCM) that can reproduce the stochastic properties of multiple-input/multiple output (MIMO) channels over time, frequency, and space. On the other hand, the 5G mmWave Channel Model Alliance is newly established and will establish guidelines for measurement calibration and methodology, modeling methodology, as well as parameterization in various environments and a database for channel measurement campaigns. NYU WIRELESS has conducted and published extensive urban propagation measurements at 28, 38 and 73 GHz for both outdoor and indoor channels, and has created large-scale and small-scale channel models and concepts of spatial lobes to model multiple multipath time clusters that are seen to arrive in particular directions [Rappaport 2013,Rappaport 2015, Samimi GCW2015, MacCartney 2015, Samimi EUCAP2016].

In this white paper, we present a brief overview of the channel properties for bands up to 100 GHz based on extensive measurement and ray tracing results across a multitude of bands. In addition we

present a preliminary set of channel parameters suitable for 5G simulations that are capable of capturing the main properties and trends.

2 Requirements for new channel model

The requirements of the new channel model that will support 5G operation across frequency bands up to 100 GHz are outlined below:

1. The new channel model should preferably be based on the existing 3GPP 3D channel model [3GPP TR36.873] but with extensions to cater for additional 5G modeling requirements and scenarios, for example:

    a. Antenna arrays, especially at higher-frequency millimeter-wave bands, will very likely be 2D and dual-polarized both at the access point (AP) and the user equipment (UE) and will hence need properly-modeled azimuth and elevation angles of departure and arrival of multipath components.

    b. Individual antenna elements will have antenna radiation patterns in azimuth and elevation and may require separate modeling for directional performance gains. Furthermore, polarization properties of the multipath components need to be accurately accounted for in the model.

2. The new channel model must accommodate a wide frequency range up to 100 GHz. The joint propagation characteristics over different frequency bands will need to be evaluated for multi-band operation, e.g., low-band and high-band carrier aggregation configurations.

3. The new channel model must support large channel bandwidths (up to 2GHz), where:

    a. The individual channel bandwidths may be in the range of 100 MHz to 2 GHz and may support carrier aggregation.

    b. The operating channels may be spread across an assigned range of several GHz

4. The new channel model must support a range of large antenna arrays, in particular:

    a. Some large antenna arrays will have very high directivity with angular resolution of the channel down to around 1.0 degree.

    b. 5G will consist of different array types, e.g., linear, planar, cylindrical and spherical arrays, with arbitrary polarization.

    c. The array manifold vector can change significantly when the bandwidth is large relative to the carrier frequency. As such, the wideband array manifold assumption is not valid and new modeling techniques may be required. It may be preferable, for example, to model arrival/departure angles with delays across the array and follow a spherical wave assumption instead of the usual plane wave assumption.

5. The new channel model must accommodate mobility, in particular:

a. The channel model structure should be suitable for mobility up to 350 km/hr.

b. The channel model structure should be suitable for small-scale mobility and rotation of both ends of the link in order to support scenarios such as device to device (D2D) or vehicle to vehicle (V2V).

6. The new channel model must ensure spatial/temporal/frequency consistency, in particular:

   a. The model should provide spatial/temporal/frequency consistencies which may be characterized, for example, via spatial consistence, inter-site correlation, and correlation among frequency bands.

   b. The model should also ensure that the channel states, such as Line Of Sight (LOS)/non-LOS (NLOS) for outdoor/indoor locations, the second order statistics of the channel, and the channel realizations change smoothly as a function of time, antenna position, and/or frequency in all propagation scenarios.

   c. The spatial/temporal/frequency consistencies should be supported for simulations where the channel consistency impacts the results (e.g. massive MIMO, mobility and beam tracking, etc.). Such support could possibly be optional for simpler studies.

7. The new channel model must be of practical computational complexity, in particular:

   a. The model should be suitable for implementation in single-link simulation tools and in multi-cell, multi-link radio network simulation tools. Computational complexity and memory requirements should not be excessive. The 3GPP 3D channel model [3GPP TR36.873] is seen, for instance, as a sufficiently accurate model for its purposes, with an acceptable level of complexity. Accuracy may be provided by including additional modeling details with reasonable complexity to support the greater channel bandwidths, and spatial and temporal resolutions and spatial/temporal/frequency consistency, required for millimeter-wave modeling.

   b. The introduction of a new modeling methodology (e.g. Map based model) may significantly complicate the channel generation mechanism and thus substantially increase the implementation complexity of the system-level simulator. Furthermore, if one applies a completely different modeling methodology for frequencies above 6 GHz, it would be difficult to have meaningful comparative system evaluations for bands up to 100 GHz.

3 Typical Deployment Scenarios

The traditional modeling scenarios (UMa, UMi and indoor hotspot (InH)) have previously been considered in 3GPP for modeling of the radio propagation in bands below about 6 GHz. The new channel model discussed in this paper is for a selective set of 5G scenarios and encompasses the following cases:

3.1 Urban Micro (UMi) Street Canyon and Open Square with outdoor to outdoor (O2O) and outdoor to indoor (O2I)

Figure 1. UMi Street Canyon

Figure 2. UMi Open Square

A typical UMi scenario is shown for street canyon and open square in Figure 1 and Figure 2, respectively. The cell radii for UMi is typically less than 100 m and the access points (APs) are mounted below rooftops (e.g., 3-20 m). The UEs are deployed outdoor at ground level or indoor at all floors.

3.2 Indoor (InH)– Open and closed Office, Shopping Malls

The indoor scenario includes open and closed offices, corridors within offices and shopping malls as examples. The typical office environment has open cubicle areas, walled offices, open areas, corridors, etc., where the partition walls are composed of a variety of materials like sheetrock, poured concrete, glass, cinder block, etc. For the office environment, the APs are mounted at a height of 2-3 m either on the ceilings or walls. The shopping malls are generally 2-5 stories high and often include an open area (“atrium”). In the shopping-mall environment, the APs are mounted at a height of approximately 3 m on the walls or ceilings of the corridors and shops. The density of the APs may range from one per floor to one per room, depending on the frequency band and output power The typical indoor office scenario and shopping malls are shown in Figure 3 and Figure 4, respectively.

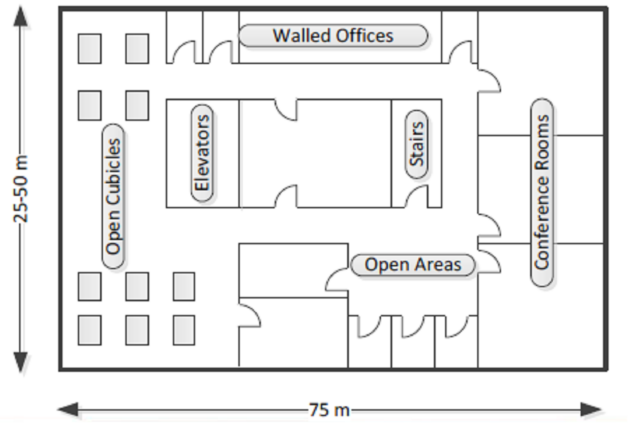

Figure 3. Typical Indoor Office

Figure 4. Indoor Shopping Malls

3.3 Urban Macro (UMa) with O2O and O2I

Figure 5. UMa Deployment

The cell radii for UMa is typically above 200 m and the APs are mounted on or above rooftops (e.g. 25-35 m), an example of which is shown in Figure 5. The UEs are deployed both outdoor at ground level and indoor at all floors.

4 Characteristics of the Channel in 6 GHz-100 GHz

Measurements over a wide range of frequencies have been performed by the co-signatories of this white paper. However, due to the more challenging link budgets at higher frequencies there are few

measurements at larger distances, e.g. beyond 200-300 m in UMi or in severely shadowed regions at shorter distances. In UMa measurements were able to be made at least in the Aalborg location at distances up to 1.24 km. An overview of the measurement and ray-tracing campaigns can be found in the Appendix. In the following sections we outline the main observations per scenario with some comparisons to the existing 3GPP models for below 6 GHz (e.g. [3GPP TR36.873]).

4.1 UMi Channel Characteristics

The LOS path loss in the bands of interest appears to follow Friis' free space path loss model quite well. Just as in lower bands, a higher path loss slope (or path loss exponent) is observed in NLOS conditions. The shadow fading in the measurements appears to be similar to lower frequency bands, while ray-tracing results show a much higher shadow fading (>10 dB) than measurements, due to the larger dynamic range allowed in some ray tracing experiments.

In NLOS conditions at frequencies below 6.0 GHz, the RMS delay spread is typically modelled at around 50-500 ns, the RMS azimuth angle spread of departure (from the AP) at around 10-30°, and the RMS azimuth angle spread of arrival (at the UE) at around 50-80° [3GPP TR36.873]. There are measurements of the delay spread above 6 GHz which indicate somewhat smaller ranges as the frequency increases, and some measurements show the millimeter wave omnidirectional channel to be highly directional in nature.

4.2 UMa Channel Characteristics

Similar to the UMi scenario, the LOS path loss behaves quite similar to free space path loss as expected. For the NLOS path loss, the trends over frequency appear somewhat inconclusive across a wide range of frequencies. The rate at which the loss increases with frequency does not appear to be linear, as the rate is higher in the lower part of the spectrum. This could possibly be due to diffraction, which is frequency dependent, being a more dominating propagation mechanism at the lower frequencies. At higher frequencies reflections and scattering may be more predominant. Alternatively, the trends could be biased by the lower dynamic range in the measurements at the higher frequencies. More measurements are needed to understand the UMa channel.

From preliminary ray-tracing studies, the channel spreads in delay and angle appear to be weakly dependent on the frequency and are generally 2-5 times smaller than in [3GPP TR36.873].

The cross-polar scattering in the ray-tracing results tends to increase (lower XPR) with increasing frequency due to diffuse scattering.

4.3 InH Channel Characteristics

In LOS conditions, multiple reflections from walls, floor, and ceiling give rise to waveguiding. Measurements in both office and shopping mall scenarios show that path loss exponents, based on a 1 m free space reference distance, are typically below 2, leading to more favorable path loss than predicted by Friis' free space loss formula. The strength of the waveguiding effect is variable and the path loss exponent appears to increase very slightly with increasing frequency, possibly due to the relation between the wavelength and surface roughness.

Measurements of the small scale channel properties such as angular spread and delay spread have shown remarkable similarities between channels over a very wide frequency range. It appears as if the

main multipath components are present at all frequencies though with some smaller variations in amplitudes.

Recent work shows that polarization discrimination ranges between 15 and 25 dB for indoor millimeter wave channels [Karttunen EuCAP2015], with greater polarization discrimination at 73 GHz than at 28 GHz [MacCartney 2015].

4.4 Penetration Loss in all Environments

4.4.1 Outdoor to indoor channel characteristics

In both the UMa and the UMi scenario a significant portion of UEs or devices are expected to be indoors. These indoor UEs increase the strain on the link budget since additional losses are associated with the penetration into buildings. The characteristics of the building penetration loss and in particular its variation over the higher frequency range is therefore of high interest and a number of recent measurement campaigns have been targeting the material losses and building penetration losses at higher frequencies [Rodriguez VTC Fall 2014], [Zhao 2013], [Larsson EuCAP 2014]. The current understanding, based on these measurements is briefly summarized as follows.

Different materials commonly used in building construction have very diverse penetration loss characteristics. Common glass tends to be relatively transparent with a rather weak increase of loss with higher frequency due to conductivity losses. "Energy-efficient" glass commonly used in modern buildings or when renovating older buildings is typically metal-coated for better thermal insulation. This coating introduces additional losses that can be as high as 40 dB even at lower frequencies. Materials such as concrete or brick have losses that increase rapidly with frequency. Figure 6 summarizes some recent measurements of material losses. The loss trends with frequency are linear to a first order of approximation. Variations around the linear trend can be understood from multiple reflections within the material or between different layers which cause constructive or destructive interference depending on the frequency and incidence angle.

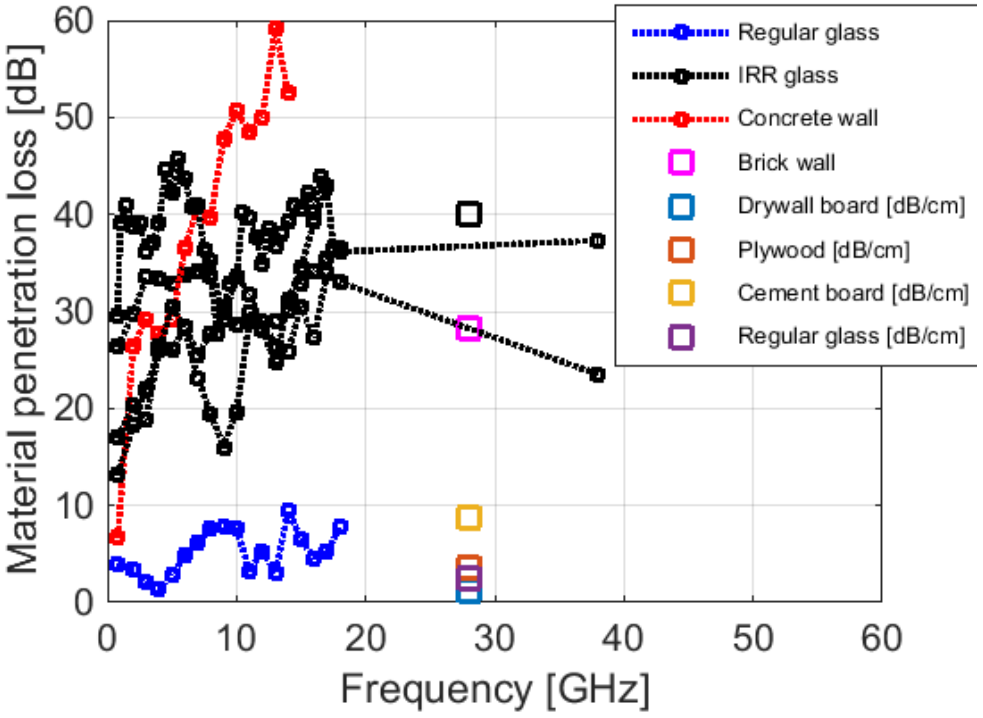

Figure 6. Measured material penetration losses. Sources: [Rodriguez VTC Fall 2014], [Zhao 2013], and measurements by Samsung and Nokia.

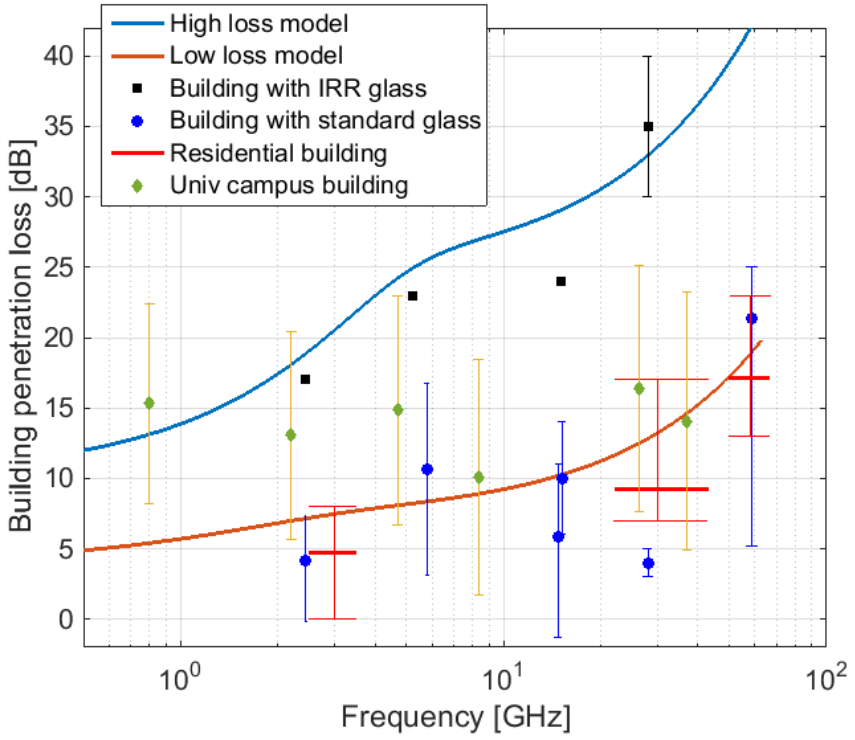

Figure 7. Effective building penetration loss measurements. The bars indicate variability for a given building. Sources: [Larsson EuCAP 2014] and measurements by Qualcomm, NTT DOCOMO, and

Ericsson. The solid curves represent two variants of the model described in [Semaan Globecomm 2015], which is one out of several penetration loss models considered in this white paper.

Typical building facades are composed of several materials, e.g. glass, concrete, metal, brick, wood, etc. Propagation of radio waves into or out of a building will in most cases be a combination of transmission paths through different materials, i.e. through windows and through the facade between the windows. The exception could be when very narrow beams are used which only illuminates a single material or when the indoor node is very close to the external wall. Thus, the effective penetration loss can behave a bit differently than the single material loss. A number of recent measurements of the effective penetration loss are summarized in Figure 7. As indicated by the bars available for some of the measurements, there can be quite some variation even in a single building. For comparison, two models that attempt to capture the loss characteristics of buildings consisting of multiple materials are shown. The loss characteristics of each specific material follows the results shown in Figure 7 quite well which indicates that the results in the material loss measurements and the effective penetration loss measurements are actually fairly consistent even though the loss values behave differently.

The majority of the results presented so far have been waves with perpendicular incidence to the external wall. As the incidence angles become more grazing the losses have been observed to increase by up to 15-20 dB.

Propagation deeper into the building will also be associated with an additional loss due to internal walls, furniture etc. This additional loss appears to be rather weakly frequency-dependent but rather strongly dependent on the interior composition of the building. Observed losses over the 2-60 GHz range of 0.2-2 dB/m.

4.4.2 Inside buildings

Measurements have been reported for penetration loss for various materials at 2.5, 28, and 60 GHz for indoor scenarios [Rappaport Book2015] [Rappaport 2013] [And 2002][Zhao 2013]. For easy comparisons, walls and drywalls were lumped into a common dataset and different types of clear class were lumped into a common dataset with normalized penetration loss shown in Figure 8. It was observed that clear glass has widely varying attenuation (20 dB/cm at 2.5 GHz, 3.5 dB/cm at 28 GHz, and 11.3 dB/cm at 60 GHz). For mesh glass, penetration was observed to increase as a function of frequency (24.1 dB/cm at 2.5 GHz and 31.9 dB/cm at 60 GHz), and a similar trend was observed with whiteboard penetration increasing as frequency increased. At 28 GHz, indoor tinted glass resulted in a penetration loss 24.5 dB/cm. Walls showed very little attenuation per cm of distance at 28 GHz (less than 1 dB/cm).

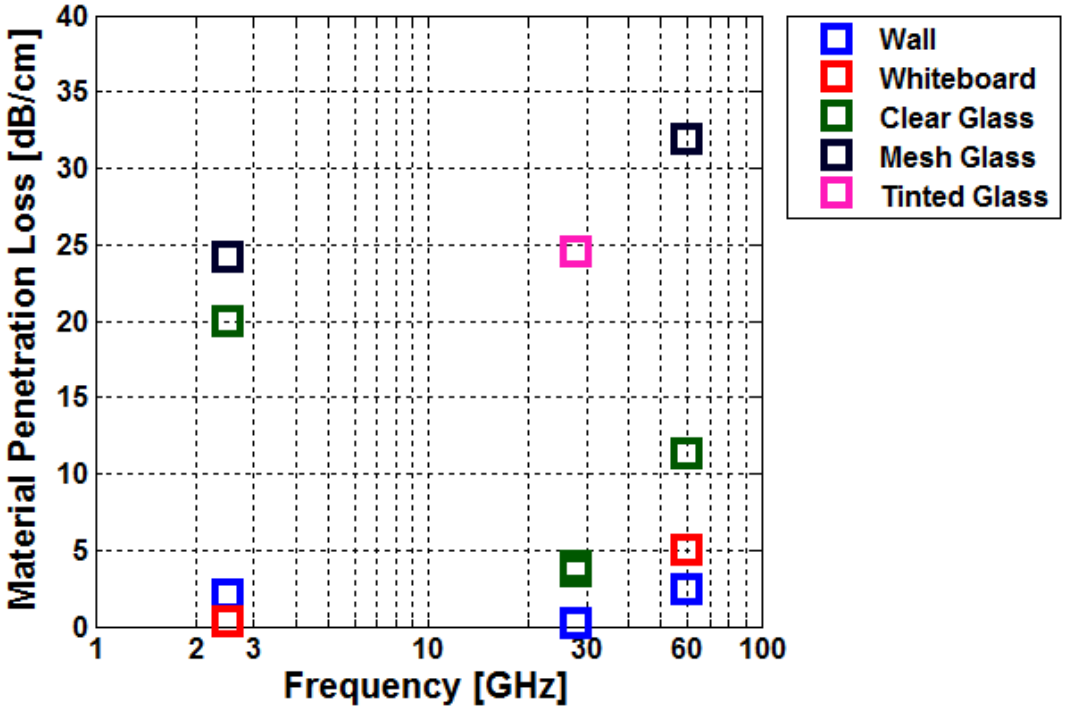

Figure 8. 2.5 GHz, 28 GHz, and 60 GHz normalized material penetration losses from indoor measurements with common types of glass and walls lumped into common datasets [Rappaport 2013] [And2002][Zhao 2013] [Nie 2013].

4.5 Blockage in all Environments

As the radio frequency increases, its propagation behaves more like optical propagation and may become blocked by intervening objects. Typically, two categories of blockage are considered: dynamic blockage and geometry-induced blockage. Dynamic blockage is caused by the moving objects (i.e., cars, people) in the communication environment. The effect is transient additional loss on the paths that intercept the moving object. Figure 9 shows such an example from 28 GHz measurement done by Fraunhofer HHI in Berlin. In these experiments, time continuous measurements were made with the transmitter and receiver on each side of the road that had on-off traffic controlled by traffic light. Note that the time periods when the traffic light is red is clearly seen in the figure as periods with little variation as the vehicles are static at that time. When the traffic light is green, the blocking vehicles move through the transmission path at a rapid pace as is seen in the figure. The variations seen when the light is red are explained by vehicles turning the corner to pass between the transmitter and receiver.

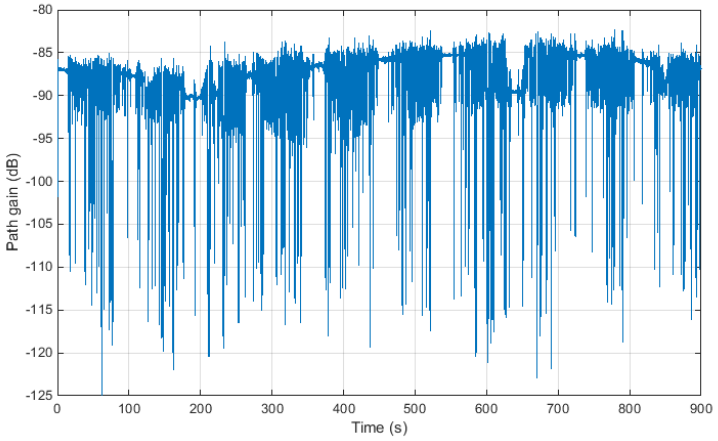

Figure 9 Example of dynamic blockage from a measurement snapshot at 28 GHz

Geometry-induced blockage, on the other hand, is a static property of the environment. It is caused by objects in the map environment that block the signal paths. The propagation channels in geometry-induced blockage locations are dominated by diffraction and sometimes by diffuse scattering. The effect is an exceptional additional loss beyond the normal path loss and shadow fading. Figure 10 illustrates examples of diffraction-dominated and reflection-dominated regions in an idealized scenario. As compared to shadow fading caused by reflections, diffraction-dominated shadow fading could have different statistics (e.g., different mean, variance and coherence distance).

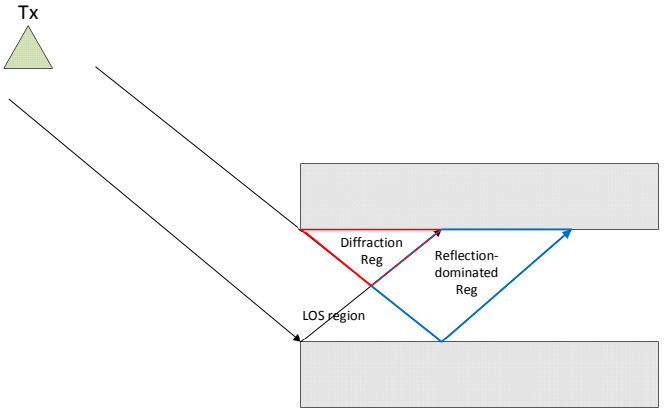

Figure 10 Example of diffraction-dominated and reflection-dominated regions (idealized scenario)

5 Channel Modeling Considerations

Table 1 summarizes a review of the 3GPP 3D channel model [3GPP TR36.873] capabilities. A plus sign "+" means that the current 3GPP 3D channel model supports the requirement, or the necessary changes are very simple. A minus sign "-" means that the current channel model does not support the requirement. This evaluation is further split into two frequency ranges: below 6 GHz and above 6 GHz. Note that in the table, LSP stands for large-scale parameter.

Table 1. Channel Modeling Considerations

Attribute	Requirement	Below 6 GHz	Above 6 GHz	Improvement addressed in this white paper	Comments
#1 Scenarios	Support of new scenarios such as indoor office, stadium, shopping mall etc.	-	-	✓	Current 3GPP model supports UMi and UMa
#2 Frequency Range	0.5 GHz – 100 GHz supported	+	-	✓	Current 3GPP model 2 – 6 GHz
	Consistency of channel model parameters between different frequency bands	-	-	×	E.g. shadowing, angle of departure, and in carrier aggregation
#3 Bandwidth	~100 MHz BW for below 6 GHz, 2 GHz BW for above 6 GHz	+	-	✓	
#4 Spatial Consistency	Spatial consistency of LSPs with fixed BS	+	-	×	LSP map (2D or 3D)
	Spatial consistency of LSPs with arbitrary Tx / Rx locations (D2D / V2V)	-	-	×	Complexity issue (4D or 6D map)
	Fair comparison of different network topologies	-	-	×	
	Spatial consistency of SSPs	-	-	×	Autocorrelation of SSPs
	UDN / MU Consistency	-	-	×	Sharing of objects / clusters
	Distributed antennas and extremely large arrays	-	-	×	
	Dynamic channel (smooth evolution of SSPs and LSPs)	-	-	×	Tx / Rx / scatterer mobility Possible methods

					for modeling varying DoDs and DoAs are discussed in the Appendix
#5 Large Array Support	Spherical wave	-	-	×	Also far field spherical
	High angular resolution down to 1 degree	-	-	×	Realistic PAS?
	Accurate modeling of Laplacian PAS	-	-	×	20 sinusoids problem
	Very large arrays beyond consistency interval	-	-	×	
#6 Dual-mobility support (D2D, V2V)	Dual Doppler	+	-	×	Not yet done, but should be easy
	Dual angle of arrival (AoA)	+	-	×	Not yet done, but should be easy
	Dual Antenna Pattern (mobile antenna pattern at both ends of the link)	+	-	×	Not yet done, but should be easy
	Arbitrary UE height (e.g. different floors)	-	-	×	
	Spatially consistent multi-dimensional map	-	-	×	Complexity issue (4D or 6D map)
#7 LOS Probability	Spatially consistent LOS probability / LOS existence	-	-	×	
#8 Specular Reflection		?	-	×	Important in mmW
#9 Path Loss	Frequency dependent path loss model	+	-	✓	
	Power scaling (directive antennas vs.	?	-	✓	

	omnidirectional)				
	Multiple NLOS cases	?	-	✓	Important in mmW
#10 Shadowing	Log-normal shadowing	+	-	✓	Shadow fading (SF) parameters needed for high frequency
	Body shadowing	-	-	×	
#11 Blockage	Blockage modelling	-	-	✓	
#12 Cluster definition	3GPP 3D cluster is defined as fixed delay and Laplacian shape angular spread.	+	-	×	It is not guaranteed that the Laplacian shape cluster is valid for mmW.
#13 Drop concept (block stationarity)	APs and UEs are dropped in some manner (e.g., hexagonal grid for 3GPP)	+	-	×	It is not sure if the drop concept works perfectly in mmWave. Also it is not clear how to test beam tracking, for instance.
#14 Accurate LSP Correlation	Consistent correlation of LSPs is needed.	-	-	×	The current 3GPP model provides different result depending on the order of calculation (autocorrelation, cross-correlation)
#15 Number of Paths	The number of paths needs to be accurate across frequency.	+	-	×	The current model is based on low frequency measurements.
#16 Moving Environment	Cars, people, vegetation etc.	-	-	×	

#17 Diffuse Propagation	Specular vs. diffuse power ratio, modeling of diffuse scattering	+	-	×	Most mmW measurements report specular only despite the fact that diffuse exists

6 Pathloss, Shadow Fading, LoS and Blockage Modeling

6.1 LOS probability

The definition of LOS used in this white paper is discussed in this sub-section together with other LOS models. The LOS state is determined by a map-based approach, i.e., by considering the transmitter (AP) and receiver (UE) positions and whether any buildings or walls are blocking the direct path between the AP and the UE. The impact of objects not represented in the map such as trees, cars, furniture, etc. is modelled separately using shadowing/blocking terms. An attractive feature of this LOS definition is that it is frequency independent , as only buildings and walls are considered in the definition.

The first LOS probability model considered, the d_1/d_2 model, is the current 3GPP/ITU model [3GPP TR36.873] [ITU M.2135-1]:

$$p(d) = \min\left(\frac{d_1}{d},1\right)\left(1-e^{-d/d_2}\right)+e^{-d/d_2}, \quad (1)$$

where d is the 2D distance in meters and d_1 and d_2 can both be optimized to fit a set of data (or scenario parameters).

The next LOS probability model considered, the NYU (squared) model, is the one developed by NYU in [Samimi 2015]:

$$p(d) = \left(\min\left(\frac{d_1}{d},1\right)\left(1-e^{-d/d_2}\right)+e^{-d/d_2}\right)^2, \quad (2)$$

where again d_1 and d_2 can be optimized to fit a given set of data (or scenario parameters).

An investigation into the LOS probability for the UMa environment was conducted using all of the UMa measured and ray tracing data listed in the appendix. In addition to comparing the two models considered above with optimized d_1 and d_2 values, the data was also compared to the current 3GPP UMa LOS probability model (eqn (1)) for a UE height of 1.5 m with d_1=18 and d_2=63. A summary of the results is given in Table 2 and the three models are compared to the data in Figure 11. In terms of mean squared error (MSE) between the LOS probability from the data and the models, the NYU (squared) model had the lowest MSE, but the difference was small. Given that the current 3GPP UMa model was a reasonable match to the data and included support for 3D placement of UEs, it is recommended that the current 3GPP LOS probability model for UMa be used for frequencies above 6.0 GHz. The 3GPP Uma model specifically is [3GPP TR36.873]:

$$p(d) = \left(\min\left(\frac{18}{d}, 1\right)\left(1 - e^{-d/63}\right) + e^{-d/63} \right)\left(1 + C(d, h_{UT})\right), \tag{3}$$

where h_{UT} is the height of the UE in m and:

$$C(d, h_{UT}) = \begin{cases} 0, & h_{UT} < 13\,m \\ \left(\frac{h_{UT} - 13}{10}\right)^{1.5} g(d), & 13 \le h_{UT} \le 23\,m \end{cases}, \tag{4}$$

$$g(d) = \begin{cases} (1.25e^{-6}) d^2 \exp\left(-d/150\right), & d > 18\,m \\ 0, & otherwise \end{cases}, \tag{5}$$

Note that for indoor users d is replaced by the 2D distance to the outer wall.

Table 2. Comparison of the LOS probability models for the UMa environment

	d1	d2	MSE
3GPP UMa	18	63	0.020
d1/d2 model	20	66	0.017
NYU (squared)	20	160	0.015

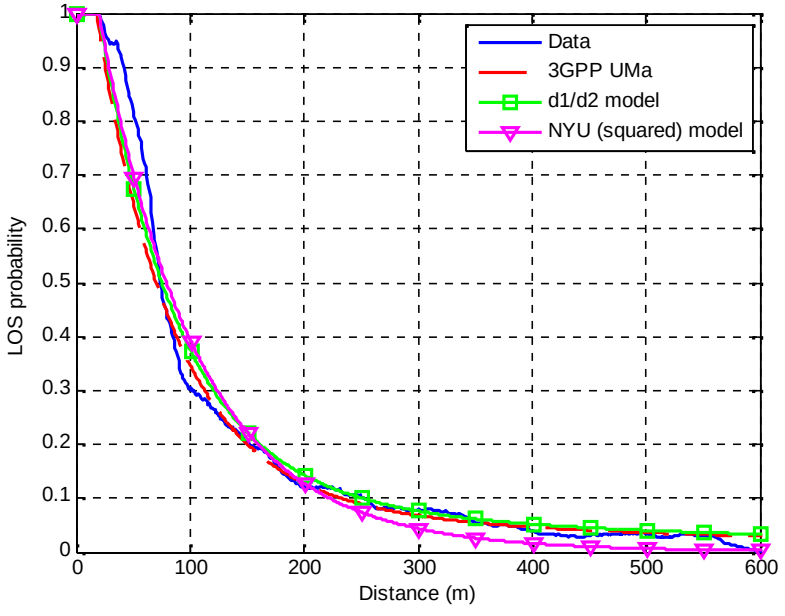

Figure 11. UMa LOS probability for the three models considered.

For the UMi scenario, it was found that the 3GPP LOS probability formula [3GPP TR36.873] is sufficient for frequencies above 6 GHz. The fitted d1/d2 model in (1) provides better fitted model, however, the errors between the data and the 3GPP LoS probability model over all distances are small. That formula is the same as (1) with d_1=18 m and d_2=36 m with d being replaced by the 2D distance

to the outer wall for indoor users. Note that the 3GPP UMi LOS probability model is not a function of UE height like the UMa LOS probability model.

Table 3. Comparison of the LOS probability models for the UMi environment

	d1	d2	MSE
3GPP UMi	18	36	0.023
d1/d2 model	20	39	0.001
NYU (squared)	22	100	0.026

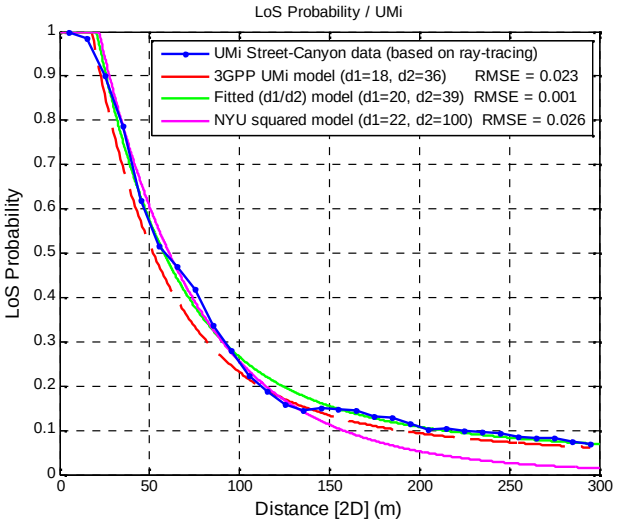

Figure 12. UMi LOS probability for the three models considered.

Since the 3GPP 3D model [3GPP TR36.873] does not include an indoor scenario, and the indoor hotspot scenario in e.g. the IMT advanced model [ITU M.2135-1] differs from the office scenario considered in this white paper, an investigation on the LOS probability for indoor office has been conducted based on ray-tracing simulation. Different styles of indoor office environment were investigated, including open-plan office with cubical area, closed-plan office with corridor and meeting room, and also hybrid-plan office with both open and closed areas. It has been verified that the following model fits the propagation in indoor office environment best of the three models evaluated.

$$P_{LOS} = \begin{cases} 1, & d \le 1.2 \\ \exp(-(d-1.2)/4.7), & 1.2 < d < 6.5 \\ \exp(-(d-6.5)/32.6)\cdot 0.32, & d \ge 6.5 \end{cases} \quad (6)$$

The verification results are shown in Table 4 and Figure 13. The LOS probability model used in ITU IMT-Advanced evaluation [ITU M.2135-1] and WINNER II [WINNER II D1.1.2] are also presented here for comparison. For the ITU and WINNER II model, parameterization results based on new data vary a lot from the original model. The results show that the new model has a good fit to the data in an average sense and can be used for 5G InH scenarios evaluation. However, note the high variability between different deployments and degrees of openness in the office area.

Table 4. Comparison of the LOS probability models for the InH environment

Models	Original	Updated/New	MSE
ITU model	$P_{LOS} = \begin{cases} 1, & d \le 18 \\ \exp\left(-\left(d-18\right)/27\right), & 18 < d < 37 \\ 0.5, & d \ge 37 \end{cases}$	$P_{LOS} = \begin{cases} 1, & d \le 1.1 \\ \exp(-(d-1)/4.9), & 1.1 < d < 9.8 \\ 0.17 & d \ge 9.8 \end{cases}$	0.0499
WINNER II model (B3)	$P_{LOS} = \begin{cases} 1, & d \le 10 \\ \exp(-(d-10)/45), & d > 10 \end{cases}$	$P_{LOS} = \begin{cases} 1, & d \le 1 \\ \exp(-(d-1)/9.4), & d > 1 \end{cases}$	0.0572
WINNER II model (A1)	$P_{LOS} = \begin{cases} 1, & d \le 2.5 \\ 1-0.9(1-(1.24-0.61\log10(d))^3)^{1/3}, & d > 2.5 \end{cases}$	$P_{LOS} = \begin{cases} 1, & d \le 2.6 \\ 1-0.9(1-(1.16-0.4\log10(d))^3)^{1/3}, & d > 2.6 \end{cases}$	0.0473
New model	N/A	$P_{LOS} = \begin{cases} 1, & d \le 1.2 \\ \exp(-(d-1.2)/4.7), & 1.2 < d < 6.5 \\ \exp(-(d-6.5)/32.6)\cdot 0.32, & d \ge 6.5 \end{cases}$	0.0449

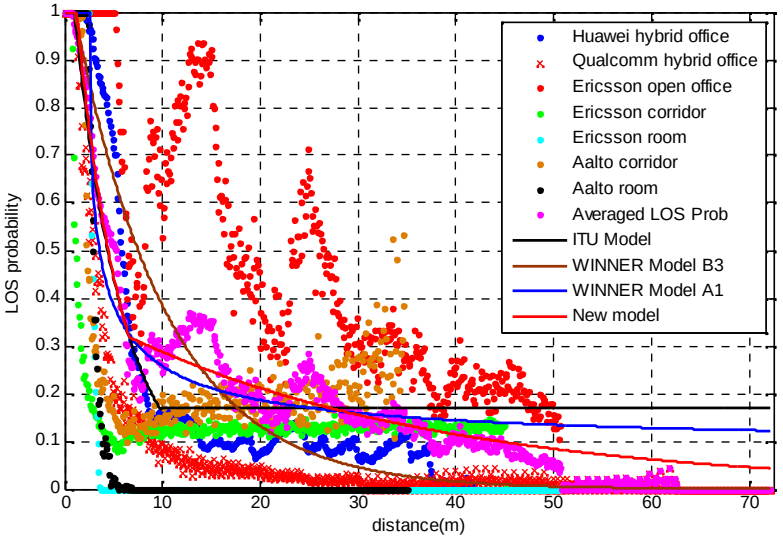

Figure 13. Indoor office LOS probability for three models considered

6.2 Path loss models

To adequately assess the performance of 5G systems, multi-frequency path loss (PL) models, LOS probability, and blockage models will need to be developed across the wide range of frequency bands and for operating scenarios. Three PL models are considered in this white paper; namely the close-in (CI) free space reference distance PL model [Andersen 1995][Rappaport 2015][SunGCW2015], the close-in free space reference distance model with frequency-dependent path loss exponent (CIF) [MacCartney 2015], and the Alpha-Beta-Gamma (ABG) PL model [Hata 1980] [Piersanti ICC2012][[MacCartney GC2013] [MacCartney 2015]. These models are described in the following text and are then applied to various scenarios. Note that the path loss models currently used in the 3GPP 3D model is of the ABG model form but with additional dependencies on base station or

terminal height, and with a LOS breakpoint. It may also be noted that the intention is to have only one path loss model (per scenario and LOS/NLOS) but that the choice is still open for discussion.

Table 5 shows the parameters of the CI, CIF, and ABG path loss models for different environments for omni-directional antennas. It may be noted that the models presented here are multi-frequency models, and the parameters are invariant to carrier frequency and can be applied across the 0.5-100 GHz band.

The CI PL model is given as [Rappaport 2015][MacCartney 2015] [SunGCW2015]

$$\mathrm{PL}^{CI}(f,d)[dB] = \mathrm{FSPL}(f,1\,m) + 10n\log_{10}\left(\frac{d}{1\,m}\right) + X_{\sigma}^{CI}, \quad (7)$$

where f is the frequency in Hz, n is the PLE, d is the distance in *meters*, X_{σ}^{CI} is the shadow fading (SF) term in dB, and the free space path loss (FSPL) at 1 m, and frequency f is given as:

$$\mathrm{FSPL}(f,1\,m) = 20\log_{10}\left(\frac{4\pi f}{c}\right), \quad (6)$$

where c is the speed of light.

The ABG PL model is given as :

$$\mathrm{PL}^{ABG}(f,d)[dB] = 10\alpha\log_{10}(d) + \beta + 10\gamma\log_{10}(f) + X_{\sigma}^{ABG}, \quad (7)$$

where α captures how the PL increase as the transmit-receive in distance (in meters) increases, β is a the floating offset value in dB, γ captures the PL variation over the frequency f in GHz,, and X_{σ}^{ABG} is the SF term in dB.

The CIF PL model is an extension of the CI model, and uses a frequency-dependent path loss exponent given by:

$$\mathrm{PL}^{CIF}(f,d)[dB] = \mathrm{FSPL}(f,1\,m) + 10n\left(1 + b\left(\frac{f - f_0}{f_0}\right)\right)\log_{10}\left(\frac{d}{1\,m}\right) + X_{\sigma}^{CIF} \quad (9)$$

where n denotes the path loss exponent (PLE), and b is an optimization parameter that captures the slope, or linear frequency dependency of the path loss exponent that balances at the centroid of the frequencies being modeled (e.g., path loss increases as f increases when b is positive). The term f_0 is a fixed reference frequency, the centroid of all frequencies represented by the path loss model, found as the weighed sum of measurements from different frequencies, using the following equation:

$$f_0 = \frac{\sum_{k=1}^{K} f_k N_K}{\sum_{k=1}^{K} N_K} \quad (10)$$

where K is the number of unique frequencies, and N_k is the number of path loss data points corresponding to the k^{th} frequency f_k. The input parameter f_0 represents the weighted frequencies of all measurement (or Ray-tracing) data applied to the model. The CIF model reverts to the CI model when b = 0 for multiple frequencies, or when a single frequency f = f_0 is modelled. For InH, a dual-slope path loss model might provide a good fit for different distance zones of the propagation environment. Frequency dependency is also observed in some of the indoor measurement campaigns conducted by co-authors. For NLOS, both a dual-slope ABG and dual-slope CIF model can be considered for 5G performance evaluation (they each require 5 modeling parameters to be optimized), and a single-slope CIF model (that uses only 2 optimization parameters) may be considered as a special case for InH-Office [MacCartney 2015]. The dual-slope may be best suited for InH-shopping mall or large indoor distances (greater than 50 m). The dual slope InH large scale path loss models are as follows:

Dual-Slope ABG model :

$$PL_{Dual}^{ABG}(d) = \begin{cases} \alpha_1 * 10\log_{10}(d) + \beta_1 + \gamma * 10\log10(f) & 1 < d \le d_{BP} \\ \alpha_1 * 10\log_{10}(d_{BP}) + \beta_1 + \gamma * 10\log10(f) + \alpha_2 * 10\log_{10}(\frac{d}{d_{BP}}) & d > d_{BP} \end{cases} \quad (11)$$

Dual-Slope CIF model:

$$PL_{Dual}^{CIF}(d) = \begin{cases} FSPL(f,1m) + 10n_1\left(1 + b_1\left(\frac{f - f_0}{f_0}\right)\right)\log_{10}(\frac{d}{1m}) & 1 < d \le d_{BP} \\ FSPL(f,1m) + 10n_1\left(1 + b_1\left(\frac{f - f_0}{f_0}\right)\right)\log_{10}(\frac{d_{BP}}{1m}) + 10n_2\left(1 + b_2\left(\frac{f - f_0}{f_0}\right)\right)\log_{10}(\frac{d}{d_{BP}}) & d > d_{BP} \end{cases} \quad (12)$$

In the CI PL model, only a single parameter, the path loss exponent (PLE), needs to be determined through optimization to minimize the SF standard deviation over the measured PL data set [SunGCW2015] [Sun VTCS2016] [Rappaport2015]. In the CI PL model there is an anchor point that ties path loss to the FSPL at 1 m, which captures frequency-dependency of the path loss, and establishes a uniform standard to which all measurements and model parameters may be referred. In the CIF model there are 2 optimization parameters (n and b), and since it is an extension of the CI model, it also uses a 1 m free-space close-in reference distance path loss anchor. In the ABG PL model there are three optimization parameters which need to be optimized to minimize the standard deviation (SF) over the data set, just like the CI and CIF PL models [MacCartney2015][Sun VTCS2016]. Closed form expressions for optimization of the model parameters for the CI, CIF, and ABG path loss models are given in [MacCartney 2015], where it was shown that indoor channels experience an increase in the PLE value as the frequency increases, whereas the PLE is not very frequency dependent in outdoor UMa or UMi scenarios [Rappaport 2015],[SunGCW2015],[Thomas VTCS2016],[Sun VTCS2016]. The CI, CIF, and ABG models, as well as cross-polarization forms and closed-form expressions for optimization are given for indoor channels in [MacCartney 2015].

Table 5. CI, CIF and ABG model parameters for different environments

Scenario	CI/CIF Model Parameters	ABG Model Parameters
UMa- LoS	n=2.0, SF = 4.1 dB	NA
UMa- nLoS	n=3.0, SF = 6.8 dB	α=3.4, β=19.2, γ=2.3, SF = 6.5 dB
UMi-Street Canyon-LoS	n=1.98, SF = 3.1 dB	NA
UMi-Street Canyon-nLoS	n=3.19, SF = 8.2 dB	α=3.48, β=21.02, γ=2.34, SF = 7.8 dB
UMi-Open Square-LoS	n=1.85, SF = 4.2 dB	NA
UMi-Open Square-nLoS	n=2.89, SF = 7.1 dB	α=4.14, β=3.66, γ=2.43, SF = 7.0 dB
InH-Indoor-LoS	n=1.73, SF = 3.02 dB	NA
InH-Indoor-nLoS single slope (FFS)	n=3.19, b=0.06, f_0= 24.2 GHz, SF = 8.29 dB	α=3.83, β=17.30, γ=2.49, SF = 8.03 dB
InH-Indoor-nLoS dual slope	n_1=2.51, b_1=0.12, f_0= 24.1 GHz, n_2=4.25, b_2=0.04, d_{BP} = 7.8 m, SF=7.65 dB	α_1=1.7, β_1=33.0, γ=2.49, d_{BP} = 6.90 m α_2=4.17, SF = 7.78 dB
InH-Shopping Malls-LoS	n=1.73, SF = 2.01 dB	NA
InH-Shopping Malls-nLoS single slope (FFS)	n=2.59, b=0.01, f_0= 39.5 GHz, SF = 7.40 dB	α=3.21, β=18.09, γ=2.24, SF = 6.97 dB
InH-Shopping Malls-nLoS dual slope	n_1=2.43, b_1=-0.01, f_0= 39.5 GHz, n_2=8.36, b_2=0.39, d_{BP} = 110 m, SF = 6.26 dB	α_1=2.9, β_1=22.17, γ=2.24, d_{BP} = 147.0 m α_2=11.47, SF = 6.36 dB

Note: the parameters of ABG model in the LoS conditions are not mentioned for the UMa and UMi scenarios because the α is almost identical to the PLE of the CI model, and also γ is very close to 2, which indicates free space path loss with frequency, and this is naturally assumed in both the CI and CIF models within the first meter of propagation.

6.3 Building penetration loss modelling

The building penetration loss model according to e.g. [3GPP TR36.873] consists of the following parts:

$$PL = PL_b + PL_{tw} + PL_{in} + N(0, \sigma) \quad (13)$$

where PL_b is the basic outdoor path loss given by the UMa or UMi path loss models, PL_{tw} is the building penetration loss through the external wall, PL_{in} is the inside loss dependent on the depth into

the building, and σ is the standard deviation. Several options for extending this model to cover the full frequency range of interest have been proposed, as shown in Table 6.

Table 6. Options for Penetration Loss Models

	PL_tw [dB]	σ [dB]	PL_in [dB/m]
IMT-advanced [M.2135] : Option 1	14+15*(1-cos(θ))^2	-	0.5
3GPP 3D [36.873] : Option 2	20	-	0.5
Option 3	15-20 (for 0-10 GHz) 20-25 (for 10-40 GHz) 25-30 (for 40-70 GHz)	8 9 10	- - -
Option 4	7 + 15/(1+exp(-0.45*(θ-20)))	6.81	0.5
Option 5	L_glass = 2+0.2*f L_IRRglass = 23+0.3*f L_concrete = 5+4*f Old building: -10*log10(0.3*10^-L_glass/10+0.7*10^-L_concrete/10) New building: -10*log10(0.7*10^-L_IRRglass/10+0.3*10^-L_concrete/10)	[TBD]	[0.2-2]

6.4 Blockage models

Dynamic blockage and geometry-induced blockage can be modelled by different modeling approaches. The dynamic blockage could be modelled as a component of the small scale fading by

including excess shadowing on a number of paths or clusters, as has been proposed in [METIS 2015] or [IEEE 802.11ad]. The geometry-induced blockage could be modelled as a component of the large-scale fading as additional shadow fading with certain occurrence probability.

It is worth noting that the environment also causes transient path gains by, for example, motion of surfaces or objects with strong reflections. The effects of transient path gains form dynamic shadow fading. **Figure 14** illustrates the concept of static shadow fading and dynamic shadow fading. When doing measurement in an uncontrolled environment, the measured instantaneous channel gain most likely includes dynamic shadow fading. By taking the expectation over multiple measurements at each Tx-Rx distance, the dynamic shadow fading can be averaged out. Path loss fitting based on the path gain expectation values gives the static path loss and static shadow fading as described in Section 5.b .

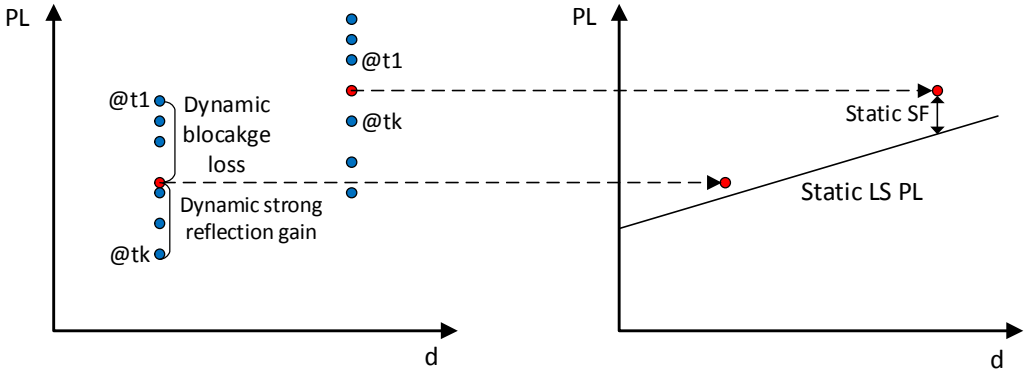

Figure 14 Illustration of static shadow fading and dynamic shadow fading

7 Fast Fading Modeling

7.1 UMi

In the double-directional channel model, the multipath components are described by the delays and the directions of departure and the direction of arrival. Each multipath component is scaled with a complex amplitude gain. Then the double-directional channel impulse response is composed of the sum of the generated double-directional multipath components. The double-directional channel model provides a complete omni-directional statistical spatial channel model (SSCM) for both LOS and NLOS scenarios in UMi environment. These results are currently analyzed based on the ray-tracing results, which is compared with the measurement campaign done in the same urban area. The final results will be derived from both the measurement and ray-tracing results.

For fast-fading modeling, ray-tracing based method is useful to extend the sparse empirical datasets and to analyze the channel characteristics in both outdoor and indoor environments. Ray-tracing results provide full information in spatio-temporal domain, which can be extracted to parameterize the double-directional channel model. Current preliminary large-scale parameters for small-scale fading model in UMi are analyzed using ray-tracing results on UMi street-canyon area in Daejeon, Korea shown in Figure 15, which models the same area conducted the measurement campaign [Hur EuCAP2015-1]. In the 3D ray-tracing simulation, the TX was placed 16 m above the ground on the

sixth-floor height and the RX was placed at 1.5 m above the ground. For the ray tracing simulations, the RX was moved on a 1 m grid in a 200 m x 200 m area. The parameters for ray-tracing simulation and environment description are similarly set to the value used in [Hur EuCAP2015-2].

Figure 15. Daejeon street canyon environments conducted measurement campaign and used for the ray-tracing study. The BS location is at the sites indicated by the star and the UEs were placed outdoors in the streets canyon areas.

The channel parameters in delay and angular domains are extracted from the ray tracing simulation. For the calculation of delay spread, the multipath components (MPCs) are cut out which power is 25 dB lower than the strongest MPC for each Tx-Rx combination. The angular spread of the mmWave channel is calculated by the elevation and azimuth angle spreads. The values of delay spread in the 28 GHz band are smaller than the values of delay spread in the conventional cellular band. This is mainly caused by the propagation characteristic of the mmWave band in a lower-scattering environment, where paths that involve effects like multiple diffractions and penetrations are more strongly attenuated. The large-scale parameters are extracted and verified that the excess delays at both 28 GHz are exponentially distributed, and azimuth angle of departure (AoD) and azimuth angle of arrival (AoA) follow a Laplacian distribution as reported in [Hur EuCAP2015-2]. For cluster-wise analysis, the K-Means algorithm [Czink VTCF06] is utilized for clustering of observed MPCs. Note that the delay scaling factor in the MCD is set to 5 and the Kim-Park (KP) index is used for determining the optimum number of clusters, following the approach in [Gustafson 2014].

After the clustering, the results from the ray-tracing simulations are analyzed in the spatio-temporal domain, for cluster parameters such as delays, angles at the TX and RX side, and the received powers. Based on the observed clusters in each link, large-scale parameters such as number of clusters and intra-cluster delay spreads and angle spreads are analyzed using the framework in [ITU M.2135-1], and all parameters are extracted by following the methodologies in [WINNER]. For further modeling purpose, the 28 GHz channel parameters of the fitted distributions for the large-scale parameters for the log-normal distribution are summarized in Appendix (Table 7. Preliminary UMi channel model parameters.

		28 GHz[1]		73 GHz[2]	
		LoS	NLoS	LoS (28-73 Combined)	NLoS
Delay spread (σ_τ) $\log_{10}$(seconds)	μ_{DS}	-8.70	-7.39	-7.71	-7.52
	ε_{DS}	0.54	0.31	0.34	0.50

AoA spread (σ_{ASA}) $\log_{10}$(degrees)	μ_{ASA}	-0.49	1.42	1.69	1.45
	ε_{ASA}	0.93	0.29	0.27	0.32
AoD spread (σ_{ASD}) $\log_{10}$(degrees)	μ_{ASD}	-0.40	0.82	1.28	1.32
	ε_{ASD}	1.07	0.38	0.50	0.38
ZoA spread (σ_{ZSA}) (degrees)	μ_{ZSA}	-1.40	0.69	0.60	0.53
	ε_{ZSA}	1.09	0.40	0.09	0.15
ZoD spread (σ_{ZSD}) (degrees)	μ_{ZSD}	-1.25	-0.21	N/A	0.46
	ε_{ZSD}	0.04	0.30	N/A	0.18
Shadow fading (dB)		0.63	22.09	3.6 (28 G) - 5.2 (73 G)	7.60
Delay distribution		Exponential distribution			
AoD and AoA distribution		Laplacian distribution		Uniform [0, 360]	
ZoD and ZoA distribution		Laplacian distribution		Gaussian distribution	
Delay scaling parameter		4.42	4.82	3.90	3.10
XPR (dB)	μ_{XPR}	TBD	TBD	TBD	TBD
	σ_{XPR}	TBD	TBD	TBD	TBD

Table 8. Preliminary UMi cluster parameters

	28 GHz[1]		73 GHz[2]	
	LoS	NLoS	LoS (28-73 Combined)	NLoS
Clustering Algorithm	K-Means algorithm		K-Means algorithm	
Ave. number of clusters	6	6	5.0	4.6
Ave. number of rays per cluster	10	10	12.4	13.2
Cluster DS (nsec)	TBD	TBD	TBD	TBD
Cluster ASA (degrees)	3.3	6.7	6.7	5.2
Cluster ASD (degrees)	2.7	5.7	1.5	2.1
Cluster ZSA (degrees)	3.9	4.9	1.8	1.5
Cluster ZSD (degrees)	1.2	1.6	N/A	0.8
Per-cluster shadow fading (dB)	5	5	13.6	17.4

Table 9. Preliminary UMi correlations for large-scale parameters

	28 GHz[1]		73 GHz[2]	
	LoS	NLoS	LoS(28-73 Combined)	NLoS
ASD vs. DS	-0.25	0.37	0.32	0.054
ASA vs. DS	0.35	0.43	0.49	0.282
ASA vs. SF	-0.01	0.03	0.54	0.042
ASD vs. SF	-0.24	0.16	-0.04	0.009
DS vs. SF	0.22	0.30	0.35	-0.177

ASD vs. ASA	-0.67	0.09	0.72	-0.256
ZSD vs. SF	0.23	0.13	N/A	-0.430
ZSA vs. SF	0.16	0.10	0.16	-0.389
ZSD vs. DS	0.27	0.50	N/A	0.950
ZSA vs. DS	0.14	0.19	0.44	0.108
ZSD vs. ASD	-0.32	0.36	N/A	0.49
ZSA vs. ASD	-0.39	0.10	0.95	-0.263
ZSD vs. ASA	0.33	0.20	N/A	0.950
ZSA vs. ASA	0.37	0.02	0.72	0.232
ZSD vs. ZSA	0.92	0.52	N/A	-0.960

1. From Samsung based on ray-tracing
2. From NYU based on measurement [Samimi EUCAP2016]

through 错误!未找到引用源。). Note that the modeling of elevation angles extending to 3D channel follows the one in [3GPP TR36.873]. It is also observed that the mean and the STD of ZSD still have a distance-dependency that decreases as the RX goes far from the TX with a breakpoint in a single-slope and a constant value.

7.2 UMa

Similar to UMi, preliminary UMa large-scale fading parameters in UMa environment were determined using ray tracing study performed in Aalborg, Denmark as shown in Figure 16. This environment was chosen as there were real-world measurements also made in the same area [Nguyen16]. Specifically there was one AP used in the study which had a height of 25 m. The UE height was 1.5 m and isotropic antennas were employed at both the AP and UE. Note that no other objects, such as vehicles, trees, light poles, and signs, were included in this ray tracing study but would be present when measurements were taken. The maximum number of rays in the simulation was 20, no transmissions through buildings were allowed, the maximum number of reflections was four, the maximum number of diffractions was one for frequencies above 10 GHz and was two for frequencies of 10 GHz and below.. Six frequencies were considered in this study, i.e., 5.6, 10, 18, 28, 39.3, and 73.5 GHz.

The preliminary large-scale parameters found for the NLOS UMa environment are given in the Appendix (Table 10 - Table 12). The delay and azimuth angle spreads were found to decrease in frequency. The large-scale parameter that seemed most affected by carrier frequency was the cross-polarization discrimination ratio (XPR), which varied from 13.87 to 7.89 dB when going from 5.6 GHz to 73.5 GHz. The drop in the ray tracing results as frequency increases was primarily attributed to diffuse scattering, as the smaller wavelength of the higher frequency sees an increase in diffuse scattering relative to the lower frequencies, which tends to depolarize the rays. It should be

noted that at this point the increasing trend of depolarization at the higher frequencies needs to be verified through measurements.

Finally, an investigation into the clustering of the rays in this ray-tracing study was performed. To determine clusters, the K-Means algorithm [Czink VTCF06] was employed with p=0.98 and s=0.95 in the shape pruning algorithm. Since this version of the K-Means algorithm has a random starting point (i.e., the first step is a random choosing of the starting centroid positions), the K-Means algorithm was ran 50 times with different random starting points and the cluster set kept at the end was the one which produced the minimum number of clusters. The results showed that the average number of clusters and the average number of rays per cluster were both fairly consistent across the different carrier frequencies. However, the cluster delay and azimuth angle spreads tended to decrease with increasing frequency. In interpreting these results, especially the average number of rays per cluster, it should be noted that the number of modelled rays was limited to 20 in the simulations,

Figure 16. Aalborg, Denmark environment used for ray-tracing study. The AP (Tx) location was at the site indicated and UEs were placed outdoors in the streets and open areas.

7.3 InH

For InH scenarios, an investigation of fast fading modelling has been conducted based on both measurement and ray-tracing. Both indoor office and shopping mall environments have been investigated at frequencies including 20 GHz, 28 GHz, 60GHz, and 73 GHz. Some preliminary analysis on large-scale channel characteristics have been summarized in Table 13. Although it is still too early to apply these results to the full frequency range up to 100 GHz, these preliminary investigations have provided insight into the difference induced by the largely extended frequency range.

7.4 O2I channel modelling

Since there is very limited data available on the O2I channel characteristics at higher frequencies it is proposed to use the same channel modeling approach and parameters as the O2O for UMa and UMi respectively. This would make the additional building penetration loss the only difference between

O2O and O2I. Possibly some smaller changes could be considered such as having a smaller elevation spread at the terminal for O2I.

APPENDIX

a. Overview of measurement campaigns

The basis for this white paper is the open literature in combination with recent and ongoing propagation channel measurements performed by the cosignatories of this white paper, some of which are as yet unpublished. The following tables give an overview of these recent measurement activities in different frequency bands and scenarios.

i. UMi street canyon O2O

Band	Party	GHz	Pathloss & Shadowing	Large Scale Parameters	Small Scale Parameters
< 30 GHz	NYU	1.8	●	●	●
	CMCC	6	●	●	Aug.
	DCM	8	●		
	CMCC	10	TBD	TBD	
	Intel	10	July.	Sep.	Sep.
	Nokia/Aalborg	2, 10, 18	●		
	CMCC	14	Sep.	Sep.	
	Aalto	15	Sep.	Sep.	Sep.
	Huawei	15			
	Ericsson	15	●	●	●
	DCM	20, 26	●	Sep. (20)	Sep. (20)
	Huawei	28	●	Nov.	Nov.
	Intel	28	Sep.	Nov.	Nov.
	NYU	28	● [Summer 2012]	● [Summer 2012]	● [Summer 2012]
	NYU	28	Sep.	Sep.	Sep.
	Samsung	28	●	●	●
	Ericsson	28			
	Nokia/Aalborg	28	●	●	
	CMCC	28	Sep.	Sep.	

	Aalto	28	●	●	●
	Qualcomm	29	Oct.	TBD	TBD

Band	Party	GHz	Pathloss & Shadowing	Large Scale Parameters	Small Scale Parameters
30 - 60 GHz	Huawei	30-40			
	DCM	37	●		
	NYU	38			
	Intel	40, 60	July (60) Sep. (40)	Sep (60) Nov. (40)	Sep. (60) Nov. (40)
	Ericsson	60			
	Huawei	60	Nov.	Nov.	Nov.
	Qualcomm	60	Oct.	TBD	TBD
> 60 GHz	Aalto	63	Sep.	Sep.	Sep.
	Huawei	73	●	Nov.	Nov.
	NYU	73	● [Summer 2013]	● [Summer 2013]	● [Summer 2013]
	Intel	75, 82	Sep.	Nov.	Nov.

ii. UMi open square O2O

Band	Party	GHz	Pathloss & Shadowing	Large Scale Parameters	Small Scale Parameters
< 30 GHz	Nokia / AAU	10	●		Madrid-grid
	CMCC	14	Sep.	Sep.	
	Nokia / AAU	2, 10,18	●		

	Nokia/AAU	28	●		
	Samsung	28	TBD (July or Sep)	TBD (Sep)	TBD (Sep)
	Qualcomm	29	●	TBD	TBD
30 - 60 GHz	Qualcomm	60	Sept	TBD	TBD
	Univ. of Bristol	60	TBD (Spring 2016)	TBD (Spring 2016)	TBD (Spring 2016)
> 60 GHz	Aalto	63	●	●	●
	NYU	73	● [Spring 2014]	● [Spring 2014]	

iii. UMi O2I

Band	Party	GHz	Pathloss & Shadowing	Large Scale Parameters	Small Scale Parameters
< 30 GHz	NYU	1.9, 5.85	●		
	DCM	8, 26	July		
	Nokia/Aalborg	10	●		
	Ericsson	6, 15, 28	●	●	●
	Nokia/Aalborg	20	●		
	Nokia/Aalborg	28	Sep.		
	Samsung	28	TBD (July)		
	NYU	28	● [Summer 2012]	● [Summer 2012]	
	Ericsson	28			

30 - 60 GHz	DCM	37	July		
	Ericsson	60	●	●	●
> 60 GHz					

iv. UMa O2O

Band	Party	GHz	Pathloss & Shadowing	Large Scale Parameters	Small Scale Parameters
< 30 GHz	CMCC	6	Sep.	Sep.	
	Nokia/Aalborg	2, 10, 18, 28	●		
	CMCC	14	TBD	TBD	
30 - 60 GHz	NYU	38	● [Summer 1998 & Summer 2011]	● [Summer 1998 & Summer 2011]	
> 60 GHz					

v. InH open-plan office

Band	Party	GHz	Pathloss & Shadowing	Large Scale Parameters	Small Scale Parameters
< 30 GHz	NYU	1.3, 1.9, 2.5, 4.0, 5.85	●	●	
	CMCC	6	Sep.	Sep.	
	CMCC	14	●	●	
	Ericsson	15			
	Huawei	15	Sept.	Nov.	Nov.
	DCM	8, 20, 26	●	Sep (20)	Sep (20)
	Huawei	28	●	Sept.	Nov.
	NYU	28	● [Summer 2012 & Summer 2014]	● [Summer 2012 & Summer 2014]	
	Samsung	28	TBD	TBD	TBD
	Ericsson	28	TBD		
	CMCC	28	Sep.	Sep.	
30 - 60 GHz	Huawei	30-40			
	DCM	37	July		
	Ericsson	60			
	NYU	60	● [2000]	● [2000]	
	Univ. of Bristol	60	TBD (Spring 2016)	TBD (Spring 2016)	TBD (Spring 2016)
	Huawei	60	Sept.	Nov.	Nov.
> 60 GH	Aalto	63, 70	●	●	●

	Huawei	72	●	Sept.	Nov.
	NYU	73	● [Spring & Summer 2014]	● [Spring & Summer 2014]	

vi. InH closed-plan office

Band	Party	GHz	Pathloss & Shadowing	Large Scale Parameters	Small Scale Parameters
< 30 GHz	NYU	1.3, 1.9, 2.5, 4.0, 5.85	●	●	
	Intel	10, 28	Sep	Nov	Nov
	Ericsson	2, 4, 6, 15	●	●	●
	NYU	28	● [Summer 2012 & Summer 2014]	● [Summer 2012 & Summer 2014]	
	Samsung	28	TBD	TBD	TBD
	Ericsson	28	TBD		
	Qualcomm	29	●	TBD	TBD
30 - 60 GHz					
	Intel	40	Sep	Nov	Nov
	Ericsson	60	●	●	●
	NYU	60	● [2000]	● [2000]	
	Qualcomm	60	July	TBD	TBD

> 60 GHz	Aalto	63, 70	●	●	●
	NYU	73	● [Spring & Summer 2014]	● [Spring & Summer 2014]	
	Intel	75, 82	Sep.	Nov	Nov

vii. InH shopping mall

Band	Party	GHz	Pathloss & Shadowing	Large Scale Parameters	Small Scale Parameters
< 30 GHz	CMCC	6	TBD	TBD	
	Nokia/Aalborg	2, 10, 18	●		
	Intel	10, 28	Sep.	Nov	Nov
	CMCC	14	Jul.	Jul.	
	Aalto	15	●	●	●
	Aalto	28	●	●	●
	Samsung	28	●	●	●
	Nokia/Aalborg	28	Sep.		
	Qualcomm	29	June	TBD	
30 - 60 GHz	Intel	40	Sep.	Nov	Nov
	Qualcomm	60	June	TBD	
	Univ. of Bristol	60	TBD (Spring 2016)	TBD (Spring 2016)	TBD (Spring 2016)
> 60 GHz	Aalto	63, 70	●	●	●
	Intel	75, 82	Sep.	Nov	Nov

b. Overview of ray-tracing campaigns

i. UMi street canyon O2O

Band	Party	GHz	Pathloss & Shadowing	Large Scale Parameters	Small Scale Parameters	Location Details
< 30 GHz	Aalto	15	Nov.	Nov.	Nov.	Greater Helsinki area
	Aalto	28	Nov.	Nov.	Nov.	Greater Helsinki area
	Samsung	28	●	●	●	Daejeon, Korea / Same location for measurement campaign
	Samsung	28	●	●	●	Ottawa
	Samsung	28	●	●	●	NYU Campus / Same location for NYU measurement campaign
	USC	28	●	●	●	
	Nokia	5.6,10.25, 28.5	●	●	●	Madrid-grid
30 - 60 GHz	Nokia	39.3	●	●	●	Madrid-grid
> 60 GHz	Aalto	63	Nov.	Nov.	Nov.	Greater Helsinki area
	Nokia	73	●	●	●	NYU Campus plus Madrid-grid

ii. UMi open square O2O

Band	Party	GHz	Pathloss & Shadowing	Large Scale Parameters	Small Scale Parameters	Location Details

< 30 GHz	Nokia	5.6,10.25, 28.5	●	●	●	Madrid-grid
	Univ. of Bristol	28	TBD (Spring 2016)	TBD (Spring 2016)	TBD (Spring 2016)	Bristol / London
30 - 60 GHz	Nokia	39.3	●	●	●	Madrid-grid
	Univ. of Bristol	40 / 60	TBD (Spring 2016)	TBD (Spring 2016)	TBD (Spring 2016)	Bristol / London
> 60 GHz	Aalto	63	●	●	●	Helsinki city center
	Nokia	73.5	●	●	●	Madrid-grid

iii. UMa O2O

Band	Party	GHz	Pathloss & Shadowing	Large Scale Parameters	Small Scale Parameters	Location Details
< 30 GHz	Nokia	5.6,10.25, 28.5	●	●	●	Madrid-grid
	Nokia/Aalborg	10, 18, 28	Sep.	Sep.	Oct.	Aalborg (same location as measurement campaigns)
	Samsung	28	●	●	●	Ottawa
	Samsung	28	●	●	●	NYU Campus
	Univ. of Bristol	28	TBD (Spring 2016)	TBD (Spring 2016)	TBD (Spring 2016)	Bristol / London

30 - 60 GHz	Univ. of Bristol	40 / 60	TBD (Spring 2016)	TBD (Spring 2016)	TBD (Spring 2016)	Bristol / London
	Nokia/Aalborg	39.3	Sep.	Sep.	Oct.	Aalborg (same location as measurement campaigns)
	Nokia	39.3	●	●	●	Madrid-grid
> 60 GHz	Nokia/Aalborg	73.5	Sep.	Sep.	Oct.	Aalborg (same location as measurement campaigns)
	Nokia	73.5	●	●	●	Madrid-grid

iv. InH open-plan office

Band	Party	GHz	Pathloss & Shadowing	Large Scale Parameters	Small Scale Parameters	Location Details
< 30 GHz	Samsung	28	TBD	TBD	TBD (Sep)	Open-Office
30 - 60 GHz						

> 60 GHz	Nokia	73	●	●	●	Open-office at NYU campus

v. InH closed-plan office

Band	Party	GHz	Pathloss & Shadowing	Large Scale Parameters	Small Scale Parameters	Location Details
< 30 GHz						
30 - 60 GHz						
> 60 GHz	Aalto	63, 70	●	●	●	Large office, meeting room, cafeteria

vi. InH shopping mall

Band	Party	GHz	Pathloss & Shadowing	Large Scale Parameters	Small Scale Parameters	Location Details

< 30 GHz	Samsung	28	TBD	TBD	TBD (Sep)	Shopping-mall like environment / Same location for measurement campaign
30 - 60 GHz						
> 60 GHz	Aalto	63, 70	●	●	●	A shopping mall in Helsinki area

c. Fast Fading Models

UMi

Table 7. Preliminary UMi channel model parameters.

		28 GHz[1]		73 GHz[2]	
		LoS	NLoS	LoS (28-73 Combined)	NLoS
Delay spread (σ_τ) $\log_{10}$(seconds)	μ_{DS}	-8.70	-7.39	-7.71	-7.52
	ε_{DS}	0.54	0.31	0.34	0.50
AoA spread (σ_{ASA}) $\log_{10}$(degrees)	μ_{ASA}	-0.49	1.42	1.69	1.45
	ε_{ASA}	0.93	0.29	0.27	0.32
AoD spread (σ_{ASD}) $\log_{10}$(degrees)	μ_{ASD}	-0.40	0.82	1.28	1.32
	ε_{ASD}	1.07	0.38	0.50	0.38
ZoA spread (σ_{ZSA}) (degrees)	μ_{ZSA}	-1.40	0.69	0.60	0.53
	ε_{ZSA}	1.09	0.40	0.09	0.15

ZoD spread (σ_{ZSD}) (degrees)	μ_{ZSD}	-1.25	-0.21	N/A	0.46
	ε_{ZSD}	0.04	0.30	N/A	0.18
Shadow fading (dB)		0.63	22.09	3.6 (28 G) - 5.2 (73 G)	7.60
Delay distribution		Exponential distribution			
AoD and AoA distribution		Laplacian distribution		Uniform [0, 360]	
ZoD and ZoA distribution		Laplacian distribution		Gaussian distribution	
Delay scaling parameter		4.42	4.82	3.90	3.10
XPR (dB)	μ_{XPR}	TBD	TBD	TBD	TBD
	σ_{XPR}	TBD	TBD	TBD	TBD

Table 8. Preliminary UMi cluster parameters

	28 GHz[1]		73 GHz[2]	
	LoS	NLoS	LoS (28-73 Combined)	NLoS
Clustering Algorithm	K-Means algorithm		K-Means algorithm	
Ave. number of clusters	6	6	5.0	4.6
Ave. number of rays per cluster	10	10	12.4	13.2
Cluster DS (nsec)	TBD	TBD	TBD	TBD
Cluster ASA (degrees)	3.3	6.7	6.7	5.2
Cluster ASD (degrees)	2.7	5.7	1.5	2.1
Cluster ZSA (degrees)	3.9	4.9	1.8	1.5
Cluster ZSD (degrees)	1.2	1.6	N/A	0.8
Per-cluster shadow fading (dB)	5	5	13.6	17.4

Table 9. Preliminary UMi correlations for large-scale parameters

	28 GHz[1]		73 GHz[2]	
	LoS	NLoS	LoS(28-73 Combined)	NLoS
ASD vs. DS	-0.25	0.37	0.32	0.054
ASA vs. DS	0.35	0.43	0.49	0.282
ASA vs. SF	-0.01	0.03	0.54	0.042
ASD vs. SF	-0.24	0.16	-0.04	0.009
DS vs. SF	0.22	0.30	0.35	-0.177
ASD vs. ASA	-0.67	0.09	0.72	-0.256
ZSD vs. SF	0.23	0.13	N/A	-0.430
ZSA vs. SF	0.16	0.10	0.16	-0.389
ZSD vs. DS	0.27	0.50	N/A	0.950
ZSA vs. DS	0.14	0.19	0.44	0.108
ZSD vs. ASD	-0.32	0.36	N/A	0.49

ZSA vs. ASD	-0.39	0.10	0.95	-0.263
ZSD vs. ASA	0.33	0.20	N/A	0.950
ZSA vs. ASA	0.37	0.02	0.72	0.232
ZSD vs. ZSA	0.92	0.52	N/A	-0.960

3. From Samsung based on ray-tracing
4. From NYU based on measurement [Samimi EUCAP2016]

UMa

Table 10. Preliminary UMa NLOS channel model parameters.

		5.6 GHz	10 GHz	18 GHz	28 GHz	39.3 GHz	73.5 GHz
Delay spread (σ_τ) $\log_{10}$(seconds)	μ_{DS}	-6.75	-6.80	-6.85	-6.88	-6.89	-6.91
	ε_{DS}	0.68	0.88	0.78	0.73	0.73	0.69
AoA spread (σ_{ASA}) $\log_{10}$(degrees)	μ_{ASA}	1.34	1.14	1.14	1.15	1.14	1.09
	ε_{ASA}	0.81	1.14	1.01	0.94	0.91	0.87
AoD spread (σ_{ASD}) $\log_{10}$(degrees)	μ_{ASD}	0.87	0.67	0.74	0.75	0.78	0.82
	ε_{ASD}	0.81	1.35	1.05	1.16	1.06	0.93
ZoA spread (σ_{ZSA}) $\log_{10}$(degrees)	μ_{ZSA}	0.48	0.31	0.26	0.26	0.24	0.20
	ε_{ZSA}	0.75	0.92	0.85	0.81	0.81	0.79
ZoD spread (σ_{ZSD}) $\log_{10}$(degrees)	μ_{ZSD}	-0.26	-0.24	-0.22	-0.22	-0.20	-0.16
	ε_{ZSD}	0.70	0.74	0.78	0.81	0.82	0.83
Shadow fading (dB)		9.82	10.22	10.28	10.12	10.14	9.97
Delay distribution		Exponential	Exponential	Exponential	Exponential	Exponential	Exponential
AoD and AoA distribution		Laplacian	Laplacian	Laplacian	Laplacian	Laplacian	Laplacian
ZoD and ZoA distribution		Laplacian	Laplacian	Laplacian	Laplacian	Laplacian	Laplacian
Delay scaling parameter		TBD	TBD	TBD	TBD	TBD	TBD
XPR (dB)	μ_{XPR}	13.87	12.94	10.97	10.76	9.38	7.89
	σ_{XPR}	6.12	6.36	6.80	6.57	6.60	6.38

Table 11. Preliminary UMa NLOS cluster parameters

Note that the ray tracer for the Uma scenario was run with only a total of 20 rays, so some clustering parameters, particularly the number of rays per cluster, may be low.

	5.6 GHz	10 GHz	18 GHz	28 GHz	39.3 GHz	73.5 GHz
	K-Means					
Ave. number of clusters	3.78	4.21	4.09	4.10	4.05	4.05
Ave. number of rays per cluster	5.89	4.66	4.97	5.05	5.10	5.19
Cluster DS (nsec)	77.97	56.79	57.61	50.41	49.63	50.72
Cluster ASA (degrees)	9.96	7.85	7.67	7.31	7.39	7.06
Cluster ASD (degrees)	4.54	4.46	4.53	4.32	4.27	4.28
Cluster ZSA (degrees)	3.70	2.71	2.38	2.34	2.39	2.29
Cluster ZSD (degrees)	0.69	0.85	0.84	0.81	0.83	0.85
Per-cluster shadow fading (dB)	6.12	5.86	5.82	5.67	5.46	4.87

Table 12. Preliminary UMa NLOS correlations for large-scale parameters

	5.6 GHz	10 GHz	18 GHz	28 GHz	39.3 GHz	73.5 GHz
ASD vs. DS	0.67	0.65	0.59	0.56	0.54	0.53
ASA vs. DS	0.06	0.09	0.06	0.06	0.05	0.04
ASA vs. SF	0.04	0.04	0.05	0.00	0.01	-0.04
ASD vs. SF	-0.18	-0.17	-0.22	-0.23	-0.25	-0.28
DS vs. SF	-0.05	-0.21	-0.15	-0.18	-0.20	-0.20
ASD vs. ASA	-0.02	0.01	0.07	0.07	0.05	0.07
ZSD vs. SF	-0.32	-0.39	-0.43	-0.43	-0.44	-0.47
ZSA vs. SF	0.21	0.17	0.15	0.08	0.07	-0.01
ZSD vs. DS	0.34	0.41	0.36	0.35	0.35	0.33
ZSA vs. DS	-0.26	-0.20	-0.17	-0.15	-0.17	-0.14
ZSD vs. ASD	0.73	0.72	0.73	0.73	0.74	0.75
ZSA vs. ASD	-0.33	-0.26	-0.19	-0.18	-0.15	-0.06
ZSD vs. ASA	0.08	0.16	0.25	0.27	0.27	0.30
ZSA vs. ASA	0.54	0.54	0.60	0.62	0.61	0.62
ZSD vs. ZSA	-0.08	0.01	0.06	0.09	0.14	0.25

InH

Table 13. Preliminary InH large-scale channel characteristics

		20 GHz[1]	28GHz[2]		60 GHz[2]		73GHz[3]	73GHz[4]
Scenario		Indoor office	Shopping mall		Shopping mall		Indoor office	Indoor office
		LOS	LOS	NLOS	LOS	NLOS	Hybrid	Hybrid
Delay spread (σ_τ) $\log_{10}$(seconds)	μ_{DS}	-7.33	-7.52	-7.59	-7.62	-7.45	-8.1	N/A
	ε_{DS}	0.1	0.17	0.33	0.20	0.11	0.4	N/A

Delay distribution		N/A	Exponential				Exponential	N/A
AoA spread (σ_{ASA}) $\log_{10}$(degrees)	μ_{ASA}	N/A	1.54	1.57	1.50	1.60	1.6	N/A
	ε_{ASA}	N/A	0.16	0.18	0.16	0.15	0.37	N/A
AoD spread (σ_{ASD}) $\log_{10}$(degrees)	μ_{ASD}	1.8	1.44	1.68	1.43	1.72	1.5	N/A
	ε_{ASD}	0.09	0.16	0.19	0.10	0.08	0.26	N/A
ZoA spread (σ_{ZSA}) (degrees)	μ_{ZSA}	N/A	0.87	0.68	0.86	0.67	-0.025d+1.18	N/A
	ε_{ZSA}	N/A	0.45	0.31	0.40	0.23	0.30	N/A
ZoD spread (σ_{ZSD}) (degrees)	μ_{ZSD}	0	0.75	0.95	0.74	0.88	-0.040d+1.45	N/A
	ε_{ZSD}	0.48	0.34	0.22	0.30	0.20	0.33	N/A
AoD and AoA distribution		N/A	Wrapped Gaussian				Uniform	N/A
ZoD and ZoA distribution		N/A	Laplacian				Laplacian	N/A
XPR (dB)	μ_{XPR}	N/A	16.12	14.48	16.85	16.06	15	11
	σ_{XPR}	N/A	6.22	6.26	6.62	5.34	2	6.5
LOS Ricean K factor (dB) *	μ_K	N/A	-0.18	n/a	-1.07	n/a	8	N/A
	ε_K	N/A	2.85	n/a	3.58	n/a	3	N/A

1. From DOCOMO based on measurement
2. From Aalto University based on measurement
3. From Nokia/NYU based on ray-tracing
4. From Huawei based on measurement

d. Processing Methodologies

i. Physical effects on propagation

As a consequence of shorter wavelengths as the carrier frequency increases, the radio propagation must be modelled with an understanding and consideration of a number of physical effects that occur in the real environment. A deployment scenario, perhaps involving up to a hundred meters of propagation transmission distance with short wavelengths, will encounter multiple different physical transmission effects. It is helpful if these physical effects are included in the overall transmission model to accurately reflect the behavior of the radio propagation environmental conditions.

An illustration of some of the physical effects of propagation is shown in Figure 17. This illustration may be helpful in understanding the multiple regions of physical processes that may be in the environment and affect the radio propagation.

- Zone1 (close range free space)

  Propagation is dominated by the direct path with few reflections.

- Zone 2 (LOS/scattered/waveguide)

  Propagation is dominated by the direct path and significant close reflections.

- Zone 3 (NLOS occultation scattered)

  Propagation is mainly by the reflections with some direct path energy but these are attenuated by distance.

- Zone 4 (distant NLOS)

Propagation is dominated by a small number of paths that are either not occulted or are a result of a good reflection.

- Zone 5 (too distant)

  The illustration also shows a fifth zone in which the signals have become too weak to be useful either through numerous multiple reflections, distance, corners or occultation. In this zone communications is generally impractical.

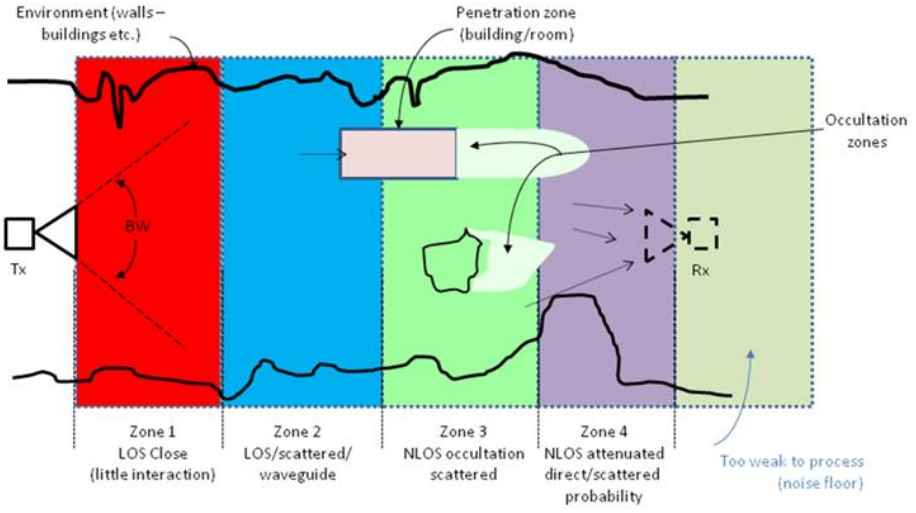

Figure 17. Illustration of multiple physical transmission effects

In each region there is always the possibility of physical blockage or occultation. Because of the small wavelengths, many typical objects in the environment (e.g. people, furniture, machinery, office equipment, etc.) are of a size that they completely block the direct signal, leaving the receiver with little except whatever reflections that may be available. This is shown in the illustration as typically in Zone 3 or 4 but it may occur anywhere. Also in some instances, there may be penetration loss for signals into interior rooms or through walls. The zone size depends on the wavelength, the dimensions and details of the environment, and the antenna beam widths. Not all zones may exist in every deployment environment or signal path. Typically, the signal propagation may experience multiple physical effects on its journey and so the "zones" may overlap in space.

ii. The effects of the antenna pattern

In understanding the measurements of the new 5G channels and the associated channel model parameters, it is helpful to know the characteristics of the antennas used to make the measurements. Some measurement antennas are directive (e.g. horn or array antennas) and consequently may not illuminate reflecting surfaces of the environment during measurements and thus may appear to simplify the environment when compared with measurements made with other non-directional antennas (e.g. omni-directional antennas). In some cases, the test antennas may have significant sidelobes in their radiation pattern and these may make the environment seem more reflective than is physically the case.

Traditionally, measurements in the frequency bands below 6 GHz have used omni-directional antennas. In these bands the transmit antenna "floods" the environment with power in all directions (i.e. sector coverage) and the receive antenna accepts power from all directions at its location. In

environments in which there are many reflections the apparent “path loss” may be reduced due to the additional power received from the many reflections. Typically in low frequency bands, the same antenna format (i.e. sector at base station and omni-directional at user equipment) is also used for the operational equipment and so the total-power/omni-directional path loss measurement is appropriate for the operating environment. Propagation studies and operation for these bands has thus been successful because the measurements, modelling and operation are all based on similar antenna characteristics.

In the bands above 6 GHz however, directional antennas (e.g. “horns”) are often used for measurements to help improve the range of the measurements. Directional antenna configurations are also expected to be used for operational equipment including mobile devices and access points as the antenna “gain” they provide may be necessary in the operational system to achieve the needed link budget. However, if the antenna configuration used for the path loss measurements is not the same as used for the operating equipment, then the associated model may not be accurate for modelling link budgets for equipment having different antenna configurations. Equipment with a narrow beam antenna will typically see less received power than would be expected based on a path loss model derived from measurements using omni-directional antennas.

a. Decoupling the antenna pattern

Many of the future systems will be operated using highly directional antennas for at least a portion of their usage. To accurately model these conditions it is necessary to decouple the channel model from the measurement antenna patterns. This is often referred to as “antenna decoupling”. The measurements are in reality the convolution of the measurement antenna patterns and the channel environment and recovering the channel environment from the measurements involves a “deconvolution” of the measuring antenna patterns from the measurements. The general process for decoupling of the antenna pattern to reconstruct the true signal angular distribution can be summarized in the following steps.

1. Estimate the path of propagation (angular domain/delay domain/both).
2. Remove the antenna pattern (different algorithms).
3. Reconstruct the estimated measured data with antenna pattern.
4. Evaluate the effect of reconstruction and antenna decoupling.

For a typical measurement antenna with a main beam and small side-lobes, the measured angular spectrum will appear as the actual channel “blurred” by the measurement antenna sampling pattern. To recover the true angular distribution of the actual channel it is necessary to undo the convolution between the measuring antenna and the channel. This is not an easy to do as practical signals and beam patterns include zeros or low amplitude regions that may prevent a simple analytical inversion from recovering the real channel. However, with sufficiently well behaved signals (i.e. with well-defined angular clusters and a good ratio between beam strength and its side-lobes) often a good approximations can be made.

Similar measurement decoupling problems are experienced in a number of other sciences and there are several algorithms for deriving the hypothetical true angular distribution from the data. Some of these processes are iterative, in which an initial estimate is gradually corrected based on its comparison to the measured data. A popular practical technique in the RADAR community is the “MUSIC” algorithm [Schmidt] while the Synthetic Aperture Imaging and radio astronomy

communities use the “CLEAN” algorithm [Clarke]. The SAGE algorithm has also been applied in this context [Fessler].

iii. Variant angles modeling for beam-tracking

A new feature for 5G communications, particularly in higher frequency bands, is that large antenna arrays or high-gain, directional antennas may be utilized in base-stations (BS) and potentially in user equipment (UE) in order to compensate for the larger propagation loss of signals above 6 GHz. The resulting beams will have small beam-widths making the transmission link sensitive to changes in angles of departure and arrival of the propagation paths between BS and UE. Modeling of the variability of angles of multipath components will enable studies of the robustness and performance evaluation of techniques such as beam-tracking. While this white paper does not provide any recommendation on the modelling methodology at this stage, it is worth mentioning some of the proposed approaches.

Variant angle model has been studied in WINNER project in [WINNER] and recently was developed to 3GPP 3D channel model with linear approximation method in [Wang2015]. Both of them are in the framework of spatial channel model (SCM) with low computational complexity. Other solutions for variant angles include the map-based channel model in METIS [METIS 2015] and the COST2100 MIMO model [Liu2012]

iv. Clustering

Different clustering algorithms were considered in support of the channel modelling activities herein described. These algorithms include the Agglomerative algorithm, the k-means algorithm and the time cluster and spatial lobe clustering algorithm.

The agglomerative algorithm is a bottom-up hierarchical clustering algorithm where multipath components (MPCs) are iteratively merged together. It starts with each MPC belonging to a different cluster and, at each step, the most similar clusters are combined. The process repeats until either a stop criterion is met or only one single cluster remains.

The K-means algorithm [Czink VTCF06] groups the multipath components (MPCs) into clusters such that the MPCs within each cluster have similar delay, elevation and azimuth angles. The algorithm identifies each cluster by its centroid position in the parameter space. Each MPC is assigned to the cluster centroid with smallest distance. The algorithm iteratively optimizes the positions of the centroids in order to minimize the total distance from each MPC to its centroid.

In the time cluster and spatial lobe clustering algorithm approach [Samimi GCW2015][Samimi ICC2015] [Samimi EUCAP2016], the time and space dimensions are considered independently, by separately performing data clustering in the temporal and spatial domains, yielding statistics for time clusters and spatial lobes in omnidirectional millimeter wave channels. Time clusters are composed of multipath components traveling close in time delay, and that arrive from potentially different angular directions in a short propagation time window as seen from field measurements. Spatial lobes represent main directions of arrival (or departure) where energy arrives over the entire time span of the multipath time delay profile. In this modeling framework, a channel impulse response “initial condition” for a particular location or point is generated by separately generating time cluster parameters and spatial lobe parameters independently, and then randomly assigning the different

multipath components to different spatial lobes as has been found to occur in millimeter wave channels.

This paper reflects the outcome from an ad-hoc industry working group that included the following participants.

Company	***Contact name***	***Email Address***
8 Aalto University	Katsuyuki Haneda	Katsuyuki.haneda@aalto.fi
BUPT	Lei Tian	tianlbupt@bupt.edu.cn
CMCC	Yi Zheng	zhengyi@chinamobile.com,
Ericsson	Henrik Asplund	henrik.aspland@ericsson.com
Huawei	Li Jian, Yi Wang, David Steer	Calvin.li@huawei.com, yi.wang@huawei.com, david.steer@huawei.com
INTEL	Clara Li, Tommaso Balercia	Clara.q.li@intel.com, tommaso.balercia@intel.com
KT Corporation	Sunguk Lee, YoungSuk Kim	Sunguk.lee@kt.com, youngsuk.kim@kt.com
Nokia	Amitava Ghosh, Tim Thomas	amitava.ghosh, @nokia.com, timothy.thomas@nokia.com
NTT DOCOMO	Takehiro Nakamura, Yuichi Kakishima, Tetsuro Imai, Haralabos Papadopoulas	nakamurata@nttdocomo.com kakishima@docomoinnovations.com imaite@nttdocomo.com hpapadopoulos@ docomoinnovations.com
NYU	Theodore (Ted) S. Rappaport, George R. MacCartney, Mathew K. Samimi, Shu Sun	tsr@nyu.edu gmac@nyu.edu mks@nyu.edu ss7152@nyu.edu
Qualcomm	Ozge Koymen	okoymen@qti.qualcomm.com
Samsung	Sooyoung Hur, Jeongho Park, Charlie Zhang	sooyoung.hur@samsung.com, jeongho.jh.park@samsung.com, jianzhong.z@samsung.com
University of Bristol	Evangelos Mellios	Evangelos.mellios@bristol.ac.uk
University of Southern California	Andreas F.Molisch	molisch@usc.edu

References

[3GPP TR25.996] 3GPP TR 25.996 (V.12.0.0), “Spatial channel model for Multiple Input Multiple Output (MIMO) simulations,” Sep. 2014.

[3GPP TR36.814] 3GPP TR 36.814 (V9.0.0), “Further advancements for E-UTRA physical layer aspects ,” Mar. 2010.

[3GPP TR36.873] 3GPP, TR 36.873 (V12.2.0), “Study on 3D channel model for LTE,” July 2015

[Andersen 1995] J. Andersen, T. Rappaport, and S. Yoshida, “Propagation measurements and models for wireless communications channels,” *IEEE Communications Magazine*, vol. 33, no. 1, pp. 42–49, Jan 1995.

[And2002] C. Anderson, et. al., “In-Building Wideband Multipath Characteristics at 2.5 & 60 GHz,” 2002 IEEE Vehicular Technology Conference, Fall 2002.

[Baum2015] D. S. Baum, J. Hansen, and J. Salo, “An interim channel model for beyond-3G systems: extending the 3GPP spatial channel model (SCM),” in Proc. IEEE VTC-spring, vol. 5, 2005, pp.3132-3136.

[Clark Sept. 1980] An efficient implementation of the algorithm 'CLEAN'; Clark, B. G.; Astronomy and Astrophysics, vol. 89, no. 3, pp377-378; Sept 1980.

[COST] http://www.cost2100.org/

[Czink VTCF06] N. Czink, et al., “A framework for automatic clustering of parametric MIMO channel data including path powers,” *in IEEE VTC-Fall 2006*, September 2006.

[ETSI 2015] ETSI, “New ETSI Group on Millimetre Wave Transmission starts work,” http://www.etsi.org/news-events/news/866-2015-01-press-new-etsi-group-on-millimetre-wave-transmission-starts-work

[Fessler VTC Fall 2014] Space-Alternating Generalized Expectation-Maximization Algorithm; Fessler, J.A.; IEEE Transactions on Signal Processing, vol. 42, no. 10, pp2664-2677; Oct 1994.

[Gustafson 2014] C. Gustafson, et. al. , “On mm-Wave Multipath Clustering and Channel Modeling,”,IEEE Transactions on Antennas and Propagation, vol. 62, no. 3, pp. 1445-1455, March 2014.

[Hata 1980] M. Hata, “Empirical formulas for propagation loss in land mobile radio service,” IEEE Trans. Veh. Technol., vol. 29, no. 3, pp. 317–325, Aug.1980

[Hur EuCAP2015-1] S. Hur, et. al.,“Wideband Spatial Channel Model in an Urban Cellular Environments At 28 GHz,” in Proc. EuCAP2015, April 2015.

[Hur EuCAP2015-2] S. Hur, et. Al., “28 GHz Channel Modeling Using 3D Ray-Tracing in Urban Environments”, in Proc. EuCAP2015, April 2015.

[ITU M.2135-1] ITU-R Rep M.2135-1, ”Guidelines for evaluation of radio interface technologies for IMT-Advanced.”

[Karttunen EuCAP2015] A. Karttunen, K. Haneda, J. Jarvelainen and J. Putkonen, “Polarisation Characteristics of Propagation Paths in Indoor 70 GHz Channels,” in Proc. 9th European Conf. Ant. Prop. (EuCAP 2015), Lisbon, Portugal, Apr. 2015.

[Larsson EuCAP 2014] C. Larsson, F. Harrysson, B-E. Olssson and J-E. Berg, "An outdoor-to-indoor propagation scenario at 28 GHz", in Proc. of European Conference on Antennas and Propagation (EuCAP) 2014, pp. 3301-3304.

[Liu2012] L. Liu, C. Oestges, J. Poutanen, K. Haneda, P. Vainikainen, F. Quitin, F. Tufvesson, P. D. Doncker, “The COST 2100 MIMO channel model,”, IEEE Wireless Communications Magazine, Dec., 2012, pp. 92-99.

[MacCartney GC2013] G. MacCartney, J. Zhang, S. Nie, and T. Rappaport, “Path loss models for 5g millimeter wave propagation channels in urban microcells,” *in 2013 IEEE Global Communications Conference (GLOBECOM)*, Dec. 2013, pp. 3948–3953.

[MacCartney 2015], G. MacCartney, et. al, “Indoor Office Wideband Millimeter-Wave Propagation Measurements and Channel Models at 28 GHz and 73 GHz for Ultra-Dense 5G Wireless Networks,” IEEE Access, October 2015.

[METIS 2013] “Simulation Guidelines,” Deliverable D6.1, METIS document number ICT-317669-METIS/D6.1, October 31, 2013.

[METIS 2015] METIS2020, Deliverable D1.4 v3, “METIS Channel Model,” July 2015. https://www.metis2020.com/wp-content/uploads/METIS_D1.4_v3.pdf

[MiWEBA 2014] MiWEBA, Deliverable D5.1 “Channel modeling and characterization,” June, 2014, http://www.miweba.eu/wp-content/uploads/2014/07/MiWEBA_D5.1_v1.011.pdf.

[mmMagic] https://5g-ppp.eu/mmmagic/

[Nie13] S. Nie, G. R. MacCartney, Jr., S. Sun, T. S. Rappaport, “72 GHz Millimeter Wave Indoor Measurements for Wireless and Backhaul Communications,” in *2013 IEEE 24th Annual International Symposium on Personal, Indoor and Mobile Radio Communications, (PIMRC)*, Sept. 2013, pp. 2429.

[NIST] http://www.nist.gov/ctl/wireless-networks/5gmillimeterwavechannelmodel.cfm

[Nguyen16] H. C. Nguyen, et al., “An Empirical Study of Urban Macro Propagation at 10, 18, and 28 GHz,” *submitted to VTC-2016/Spring*.

[Piersanti ICC2012] S. Piersanti, L. Annoni, and D. Cassioli, “Millimeter waves channel measurements and path loss models,” *in 2012 IEEE International Conference on Communications (ICC)*, June 2012, pp. 4552–4556.

[Rappaport 2013] T. S. Rappaport et al., "Millimeter Wave Mobile Communications for 5G Cellular: It Will Work!," in IEEE Access, vol.1, pp. 335-349, 2013.

[Rappaport 2015], T. S. Rappaport, et. al.," Wideband Millimeter-Wave Propagation Measurements and Channel Models for Future Wireless Communication System Design," IEEE Trans. Communications," Vol. 63, No. 9, , pp. 3029-3056, Sept. 2015.

[Rappaport Book2015] T. S. Rappaport, R. W. Heath, Jr., R. C. Daniels, and J. N. Murdock, Millimeter Wave Wireless Communications. Pearson/Prentice Hall 2015.

[Rodriguez VTC Fall 2014] I. Rodriguez, H. C. Nguyen, N. T. K. Jorgensen, T. B. Sorensen and P. Mogensen, "Radio Propagation into Modern Buildings: Attenuation Measurements in the Range from 800 MHz to 18 GHz", in Proc. of IEEE Vehicular Technology Conference (VTC fall), 2014, pp. 1-5.

[Samimi 2015] M. K. Samimi, T. S. Rappaport, and G. R. MacCartney, Jr., "Probabilistic omnidirectional path loss models for millimeter-wave outdoor communications," *in IEEE Wireless Communications Letters*, vol. 4, no. 4, pp. 357-360, Aug. 2015.

[Samimi GCW2015] M. K. Samimi, T. S. Rappaport, "3-D Statistical Channel Model for Millimeter-Wave Outdoor Communications," in 2015 IEEE Global Communications Conference, Exhibition & Industry Forum (GLOBECOM) Workshop, Dec. 6-10, 2015.

[Samimi EUCAP2016] M. K. Samimi, T. S. Rappaport, "Local Multipath Model Parameters for Generating 5G Millimeter-Wave 3GPP-like Channel Impulse Response," submitted to the 10th European Conference on Antennas and Propagation (EuCAP'2016), April 2016

[Schmidt Mar 1986] Multiple emitter location and signal parameter estimation; Schmidt, R.O. ; IEEE Transactions on Antennas and Propagation, vol. 34, Issue: 3; pp276-280; Mar1986.

[Semaan Globecom 2014] E. Semaan, F. Harrysson, A. Furuskär and H. Asplund, "Outdoor-to-indoor coverage in high frequency bands", Globecom Workshops 2014, pp. 393-398.

[Sun GCW2015], S. Sun, et. al., "Path Loss, Shadow Fading, and Line-Of-Sight Probability Models for 5G Urban Macro-Cellular Scenarios," 2015 IEEE Globecom Workshop, San Diego, Dec. 2015.

[Sun VTCS2016] S. Sun, et al., "Path Loss Models for 5G Urban Micro- and Macro-Cellular Scenarios," *submitted to IEEE VTC-Spring 2016*, May 2016.

[Tenerelli1998] P. A. Tenerelli and C. W. Bostian, "Measurement of 28 GHz diffraction loss by building corners", in Proc. IEEE PIMRC 1998, vol. 3, pp. 1166-1169, Sep. 1998.

[Thomas VTCS2016] T. Thomas, et. al., A Prediction Study of Path Loss Models from 2-73.5 GHz in an Urban-Macro Environment," *submitted to IEEE VTC-Spring 2016, May 2016.*

[Wang 2015] Y. Wang, L. Huang, Z. Shi, K. Liu, and X. Zou, "A millimeter wave channel model with variant angles under 3GPP SCM framework," in Proc. IEEE PIMRC 2015 Workshop, Hong Kong, China, Aug. 2015.]

[WINNER] WINNER II Channel Models, D1.1.2 V1.2, IST-4-027756 WINNER II Deliverable, 4 February 2008.

[Zhao 2013] H. Zhao et al.,"28 GHz millimeter wave cellular communication measurements for reflection and penetration loss in and around buildings in New York city," in 2013 IEEE International Conference on Communications (ICC), pp. 5163-5167, 9-13 June 2013.

List of Acronyms

ABG…….alpha beta gamma (path loss model)
ASA……...angle spread of arrival in azimuth (at the UE)
ASD……...angle spread of departure in azimuth (from the AP)
AP…….access point
BW……bandwidth
CI……..close in (reference-distance path loss model)
CIF……CI model with frequency-dependent path loss exponent
D2D……...device to device
DS…….delay spread
ESA……..elevation angle spread of arrival (at the UE)
ESD……..elevation angle spread of departure (from the AP)
GHz……..Giga (billion) Hertz
InH……indoor hotspot
LOS……...line of sight
LSP……large scale parameter
MIMO……...multiple input/multiple output
MSE……..mean squared error
NLOS……non line of sight
O2I……outdoor to indoor
O2O……...outdoor to outdoor
PL…….…….path loss
PLE……...path loss exponent
Rx…….receiver
SCM……..spatial channel model
SF……..shadow fading
SSCM……statistical spatial channel model
Tx……..transmitter
UE…….user equipment
UMa……..urban macro
UMi……...urban micro
V2V……...vehicle to vehicle
ZBA……..zenith (elevation) bias angle of arrival (at the UE)
ZBD……..zenith (elevation) bias angle of departure (from the AP)